Non-uniform temporal scaling of neurogenesis for species-specific dosing of cortical excitatory subtypes

Short title; Temporal scaling of rodent cortical neurogenesis

Yuki Yamauchi[1], Xuanhao D. Zhou[1], Rafat Tarfder[1], Pauline Rouillard[1], Merve Bilgic[3], Shuto Deguchi[4,5], Tomonori Nakamura[4,5,6], Yusuke Kishi[3], Kazuo Emoto[1,2], and Ikuo K. Suzuki[1]*

1. Department of Biological Sciences, Graduate School of Science, The University of Tokyo, Tokyo, Japan.
2. International Research Center for Neurointelligence, The University of Tokyo, 7-3-1 Hongo, Bunkyo-ku, Tokyo 113-0033, Japan.
3. Laboratory of Molecular Neurobiology, Institute for Quantitative Biosciences, The University of Tokyo, Tokyo 113-0032, Japan.
4. Institute for Advanced Study, Kyoto University, Yoshida-Konoe-cho, Sakyo-ku, Kyoto 606-8501, Japan.
5. Department of Anatomy and Cell Biology, Graduate School of Medicine, Kyoto University, Yoshida-Konoe-cho, Sakyo-ku, Kyoto 606-8501, Japan.
6. The Hakubi Center for Advanced Research, Kyoto University, Yoshida-Konoe-cho, Sakyo-ku, Kyoto 606-8501, Japan.

* Corresponding author:
Ikuo K. Suzuki, Ph.D.
Department of Biological Sciences, Graduate School of Science, The University of Tokyo
7-3-1 Hongo, Bunkyo-ku, Tokyo 113-0033 JAPAN
TEL: +81-3-5841-4442
Email: suzuki.ikuo@gmail.com

7. The Hakubi Center for Advanced Research, Kyoto University, Kyoto, Japan.

Abstract

Mammals share a laminar cerebral cortex, with excitatory neuron subtypes organized in distinct tangential layers. Although this framework is conserved, subtype balance varies markedly between species due to unknown mechanisms. This study shows that non-uniform scaling of temporal neurogenetic dynamics shapes species-specific neuronal composition. Comparing mice and rats, we show that rats produce more deep layer (DL) neurons but similar numbers of upper layer (UL) neurons. This difference results from a specific extension of early neurogenetic phase for DL production before transitioning to UL production in rats, as confirmed by birthdating and single-cell transcriptomics. The duration of DL production is regulated by a genetic program controlling progenitor aging, including *Ccnd1*. Knocking down *Ccnd1* in rat progenitors induces a precocious shift to UL production, mirroring the mouse pattern. Thus, while sequential cortical neurogenesis is conserved, its progression is non-uniformly scaled in each species. Such precise heterochronic fine-tuning allows evolutionary refinement of cellular configuration without drastic remodeling of the conserved corticogenesis program.

Teaser

Differential temporal progression of neural progenitor program contributes to species-specific cellular composition of mammalian cerebral cortex

MAIN TEXT

Introduction

Animals adapt their neural circuits to enhance survival in their specific ecological niches. In mammals, the cerebral cortex has evolved into a highly developed structure that supports a wide range of brain functions, culminating in advanced cognitive abilities—most notably in humans. This cortex consists of a precisely balanced repertoire of neuronal subtypes, organized into six distinct tangential layers(*1*, *2*). These layers include excitatory neuron subtypes with layer-specific roles: deep layers (DL; layers 5 and 6) primarily house extra-cortical projection neurons, layer 4 contains input-recipient neurons, and layers 2/3 consist mainly of intra-cortical projection neurons. While the diversity and laminar distribution of these excitatory subtypes are broadly conserved across mammalian species, notable quantitative variations exist and are thought to reflect functional adaptations.

However, the mechanisms that regulate the dosage and balance of these neuronal subtypes remain poorly understood. Cortical excitatory neurons are generated from radial glial (RG) progenitors—also known as apical progenitors—located in the ventricular zone (VZ). These neurons are produced in a stereotyped temporal sequence, with deep-layer neurons forming earlier than upper-layer neurons(*1*, *3–5*). Although this neurogenetic sequence is conserved among mammals, the duration and pace of each developmental stage vary widely across species(*1*, *5–10*). For example, in humans, the neurogenic period is more than ten times longer than in mice. This prolonged timeline has been linked to biological changes such as shifts in cellular metabolism(*11*). In addition, the human cortex does not expand uniformly; rather, there is a disproportionate expansion of the upper layers(*2*), which has been attributed to an extended late neurogenic phase. During this phase, various transient amplifying progenitors—including outer or basal RG—produce a surge of upper-layer neurons. Whether similar temporal adaptations underlie other interspecies differences in

cortical subtype composition remains unknown. Moreover, the specific aspects of cortical neurogenesis that are evolutionarily malleable have yet to be clarified.

Most studies on mammalian cortical evolution have focused on human-specific features, while other mammalian groups, such as rodents, remain comparatively underexplored. Rodents represent a diverse order, exhibiting a wide range of morphological, behavioral, and neural traits(*12*). Among them, mice and rats are widely used model organisms and show substantial differences in brain structure, size, and behavior. These species diverged approximately 13.1 million years ago and have since undergone distinct evolutionary adaptations. Although only a few studies have examined their divergence in detail(*13*), their widespread use in biomedical research makes them ideal candidates for comparative analysis.

In this study, we investigated cortical excitatory neurogenesis in mice and rats at single-cell resolution to uncover mechanisms underlying species-specific differences in neuronal composition. Histological analyses revealed interspecies differences in the abundance of deep-layer neurons, while upper-layer (UL; layers 2–4) neuron numbers remained comparable between species. Clonal lineage tracing from individual RG progenitors showed a species-specific increase in DL neurons, whereas UL neuron output was conserved. Combining neuronal birthdating with single-cell RNA sequencing (scRNA-seq), we demonstrate that the temporal regulation of neurogenesis by RG progenitors is scaled in a non-uniform manner between species, leading to the formation of distinct neuronal ensembles.

Results

Species-specific neuronal composition in rodent cerebral cortices; greater DL neuron numbers in rats than mice

To investigate the species-specific architecture of the rodent cerebral cortex, we performed a histological comparison of adult mice and rats (**Fig. 1** and fig. S1). Nuclear staining revealed that while the general pattern of cortical layers is conserved, a notable species difference exists in the thickness of the DL (layer 5 and 6), which are less cell-dense compared to the UL (layer 2-4) (**Fig. 1A**). The DL is significantly thicker across rostral-to-caudal cortical regions in rats than in mice (**Fig. 1A** and fig. S1B). Quantification confirmed that rats possess a greater number of DL neurons compared to mice, whereas the number of UL neurons is relatively conserved between the species (**Fig. 1B**). These findings were further supported by immunohistological staining for marker proteins specific to excitatory neuron subtypes with distinct axonal projections. Markers included Satb2 (callosal projection neurons in both UL and DL; CPN), Ctip2 (corticospinal projection neurons primarily in DL; CSPN), and Tbr1 (corticothalamic projection neurons mainly in DL; CThPN). We quantified these neuronal subtypes in the primary somatosensory cortex, identified by VGLUT2-positive barrel structures (fig. S1, C and D). Rats showed a significantly higher number of DL subtype neurons compared to mice, while the number of UL subtype neurons remained nearly identical between the two species (**Fig. 1, C and D**). These findings indicate that while mice and rats share basic cortical structures, species-specific differences are primarily observed in the abundance of DL neurons.

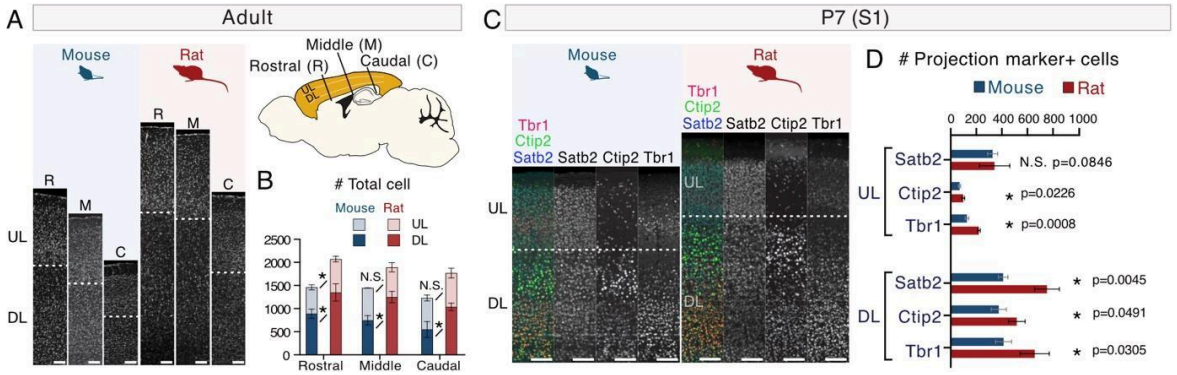

Figure 1. Histological comparison of mouse and rat cerebral cortex

(**A**) Nuclear staining of the adult mouse and rat cerebral cortex. Three rostral-to-caudal planes are defined relative to the hippocampus. White dotted lines indicate the boundary between upper layers (UL) and deep layers (DL). (**B**) Total number of DAPI-labeled nuclei in UL and DL across three rostral-to-caudal levels in both species. Statistical significance ($p < 0.05$) is indicated by asterisks. Detailed statistical data are provided in Table S2. (**C**) Detection of projection type-specific markers (Satb2, Ctip2, and Tbr1) by immunohistochemistry. White dotted lines indicate the boundary between UL and DL. (**D**) Quantification of Satb2-, Ctip2-, and Tbr1-expressing neurons in the UL and DL of the mouse and rat primary somatosensory cortex (S1) at P7. Data are presented as mean ± SEM from three samples, with p values calculated using Student's t-test. Scale bars: 100 μm (A and C).

Individual cortical RG progenitors generate species-specific number of DL neurons

Since excitatory neurons are locally supplied by RG progenitors within the same tangential position, the clonally-related sister neurons are radially clustered in a columnar space in the cerebral cortex. Previous studies using Mosaic analysis with double markers have shown that individual RG progenitors in mice generate an average of 8–9 clonal neurons, with 40–50% belonging to DL subtypes(*14*, *15*). To quantitatively compare the neuronal subtype production of individual progenitors in mice and rats in an identical methodology, we used "hemi-lineage" labeling with retroviruses expressing fluorescent reporters(*15*) (See details for hemi-lineage labeling in fig. S2, A and B). This method integrates a single copy of the retroviral vector into the host genome, permanently labeling progeny cells derived from one daughter cell of the initially infected host cell. The equally optimized titer of retroviruses expressing GFP and RFP were injected at the embryonic stage, with animals sacrificed at postnatal day 7 (P7) (**Fig. 2, A and B,** and fig. S2B), when cortical neurogenesis is complete in both species (fig. S2C). GFP- and RFP-positive cells were sparsely distributed across cortical layers without overlap between clones, confirming spatial separation of labeled clones (fig. S2B).

To compare cortical neurogenesis between the two species, we examined the transition timing of RG progenitors from proliferative to neurogenic states. At any given stage of development, RG progenitors are heterogeneous, comprising both proliferative and neurogenic subpopulations in specific ratios. The progenitor population gradually shifts from predominantly proliferative to a neurogenic mode. In mice, previous studies have shown that most cortical RG progenitors complete this transition between embryonic days E11.5 and E12.5(*14*, *15*). To identify the corresponding stage in rats, we quantified the percentage of clones containing one or two neurons, as these indicate neurogenic progenitors at the time of retroviral injection (fig. S2A). Retroviral infection at E12.5 in mice revealed that nearly half of the clones contained one or two neurons, highly consistent with earlier findings(*15*) (**Fig. 2, C and D**). A similar pattern was observed in rats when the injection was performed at E14.5 (**Fig. 2D**). In rats, neurogenic division became dominant at E15.5–E16.5, with over 50% of clones containing one or two neurons during these stages (**Fig. 2D**). These results indicate that E12.5 in mice corresponds to E14.5 in rats as the onset of neurogenesis for most cortical RG progenitors. This correspondence is further supported by conserved neuron-to-progenitor ratios identified in immunohistological analyses (fig. S2D).

Next, we compared neuron production by individual progenitors from the onset of neurogenesis (E12.5 in mice, E14.5 in rats) to P7 (**Fig. 2, B and C**). Only clones comprising three or more neurons were considered, as smaller clones likely represent incomplete lineages (fig. S2A). In mice, the mean clonal size was 6.22 ± 3.88 (median 4), consistent with previous studies(*15*) (**Fig. 2, C and E**). In contrast, clonal size distribution showed a rightward skew in rats, with a mean of 8.05 ± 5.44 (median 7) (**Fig. 2, C and E**). Neurons were categorized into DL or UL subtypes based on somal position. Rats exhibited significantly larger numbers of DL neurons per clone compared to mice (5.90 ± 4.01 in rats vs. 3.04 ± 2.69 in mice), while UL neuron numbers were similar (2.62 ± 2.98 in rats vs. 3.11 ± 2.95 in mice) (**Fig. 2F**). These results indicate that both species possess multipotent cortical RG progenitors capable of generating both DL and UL subtypes. However, neurogenic activity of each individual progenitor, particularly for DL subtype generation, is greater in rats than in mice (**Fig. 2G**).

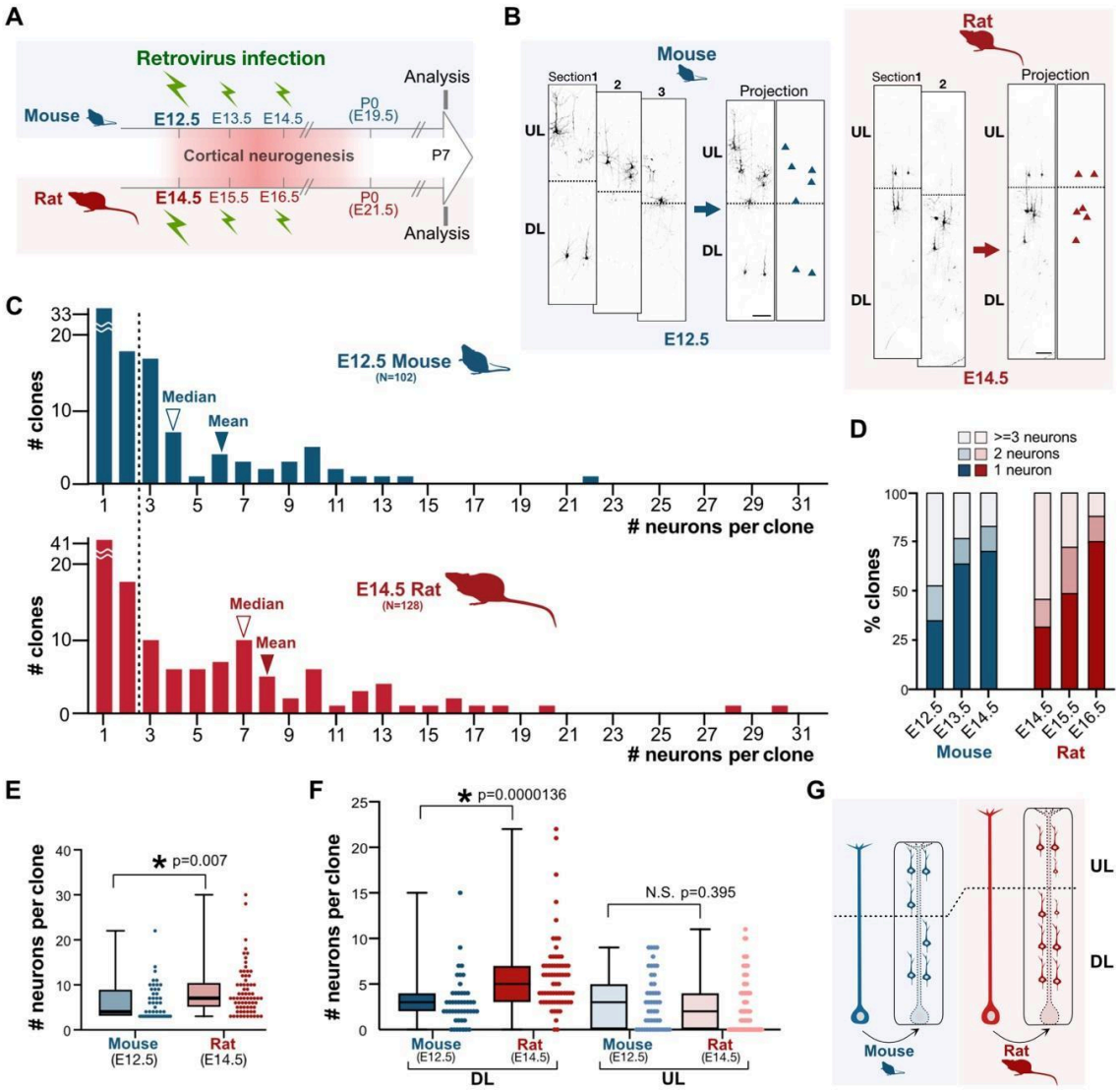

Figure 2. Clonal production of cortical excitatory neurons in mice and rats

(**A**) Time course of clonal analysis in the mouse and rat cerebral cortices. Retroviral injections were performed at the onset of neurogenesis (E12.5 in mice and E14.5 in rats), and animals were sacrificed at P7 for analysis. (**B**) Representative examples of cortical excitatory neuron clones in mice and rats. Scale bars: 100 μm. (**C**) Distribution of clone sizes when retroviruses were injected at the onset of neurogenesis. Clonal sizes represent the number of neurons generated by individual RG progenitors. Median and mean of clone size are indicated by open and filled arrowheads, respectively. (**D**) Percentage of clones containing one, two, or three or more neurons in mice and rats. (**E**) Comparison of clone size between species. Only clones with three or more neurons were analyzed. (**F**) Distributions of upper layer (UL) and deep layer (DL) neurons per clone. Rats exhibit a marked increase in the number of DL neurons per clone compared to mice, while UL neuron numbers remain similar between the species. (**G**) Schematic diagram summarizing the clonal analysis results (mean number of neurons per clone), highlighting species-specific differences in DL neuron production. Statistical analysis: p-values calculated using Student's t-test.

Species-specific timeline of cortical neurogenesis; prolonged early neurogenic phase for DL subtypes in rats than in mice

We sought to understand the mechanism underlying such a species-specific dosage of DL neuron production. An important clue was obtained by clonal analysis at different time points of retroviral injection (**Fig. 2A**, **Fig. 3** and fig. S3). Retroviruses were injected at the onset of neurogenesis ("Day 1") and 24 hours ("Day 2") and 48 hours ("Day 3") later. Progeny cells were analyzed at P7, as in the other analyses (**Fig. 3A**). The overall pattern of neurogenesis was consistent in both species. The proportion of monopotent clones containing only UL neurons increased progressively from Day 1 to Day 3, reflecting the inside-out sequence of cortical layer generation(*3*, *16*). However, a clear species-specific difference was observed: mice displayed a higher percentage of clones containing only UL neurons in injections on Days 2 and 3, while rats retained a greater proportion of multipotent clones capable of generating DL neurons, even with injections on Days 2 and 3 (**Fig. 3A**). This difference was further supported by the mean number of DL neurons per clone. In rats, DL neurons were still observed when retroviruses were injected on Day 3, whereas in mice, DL neurons were absent in the corresponding condition (**Fig. 3, A and B**). These findings suggest that cortical neurogenesis follows distinct temporal programs in the two species. In rats, the early neurogenic phase, during which DL neurons are produced, is extended through Day 3. In contrast, mice complete the transition from DL to UL neuron production by Day 3 (**Fig. 3C**).

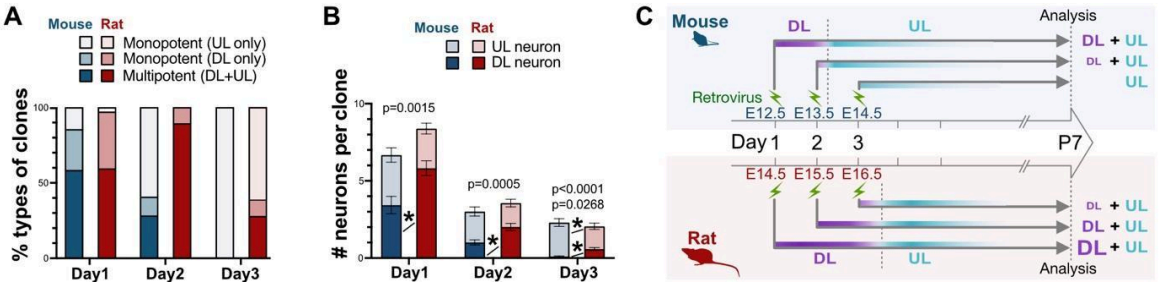

Figure 3. Temporal progression of cortical neurogenesis revealed by retroviral labeling of RG progenitors at distinct injection timings

(**A**) Clones were categorized into three types: multipotent (DL + UL), monopotent (DL only), and monopotent (UL only). By Day 3 of neurogenesis, all mouse clones were UL-only monopotent type, whereas a significant proportion of rat clones remained multipotent when retroviruses were injected at the corresponding stage. (**B**) Number of DL and UL neurons per clone after retrovirus injection at Days 1, 2, and 3 of neurogenesis in mice and rats. Rat clones contain DL neurons even at Day 3, unlike mouse clones, which transitioned entirely to UL neurons. Data are presented as mean ± SEM. Statistical significance was calculated using Student's t-test. (**C**) Summary illustration of clonal analysis with retroviral injections at different time points. Vertical dotted lines indicate the expected timing of the DL-to-UL subtype transition for the majority of RG progenitors in mice and rats.

To directly examine the timing of cortical neuron subtype generation in mice and rats, we conducted a birthdating analysis using the nucleotide analog 5-ethynyl-2'-deoxyuridine (EdU) (**Fig. 4A**). EdU was administered to label neurons undergoing their final mitosis at specific developmental stages, from the onset of neurogenesis (Day 1; E12.5 in mice and E14.5 in rats) until one day before delivery (Day 7; E18.5 in mice and E20.5 in rats). Labeled neurons were subsequently analyzed for layer positions and marker expression at P7. The analysis revealed a significant species-specific difference in neuron generation timing based on the layer positions of EdU-labeled neurons. In mice, DL neurons were generated within a two-day window (Days 1–2) before transitioning to UL neuron production. In contrast, DL neurons in rats were produced over a prolonged four-day period (Days 1–4) (**Fig. 4, B to D**). The duration of UL neurogenesis was comparable between species, lasting four days before terminating during postnatal stages. This finding was supported by the quantification of subtype-specific markers (**Fig. 4, E to H** and fig. S4). The most pronounced difference was observed in Tbr1-expressing DL neurons, which exhibited a significantly extended production period in rats compared to mice (**Fig. 4E**). These results indicate that the conserved inside-out temporal program of cortical neurogenesis is non-linearly fine-tuned in a species-specific manner. This non-uniform fine-tuning is characterized by the extended duration of DL neuron production in rats before the transition to UL neuron production (**Fig. 4I**).

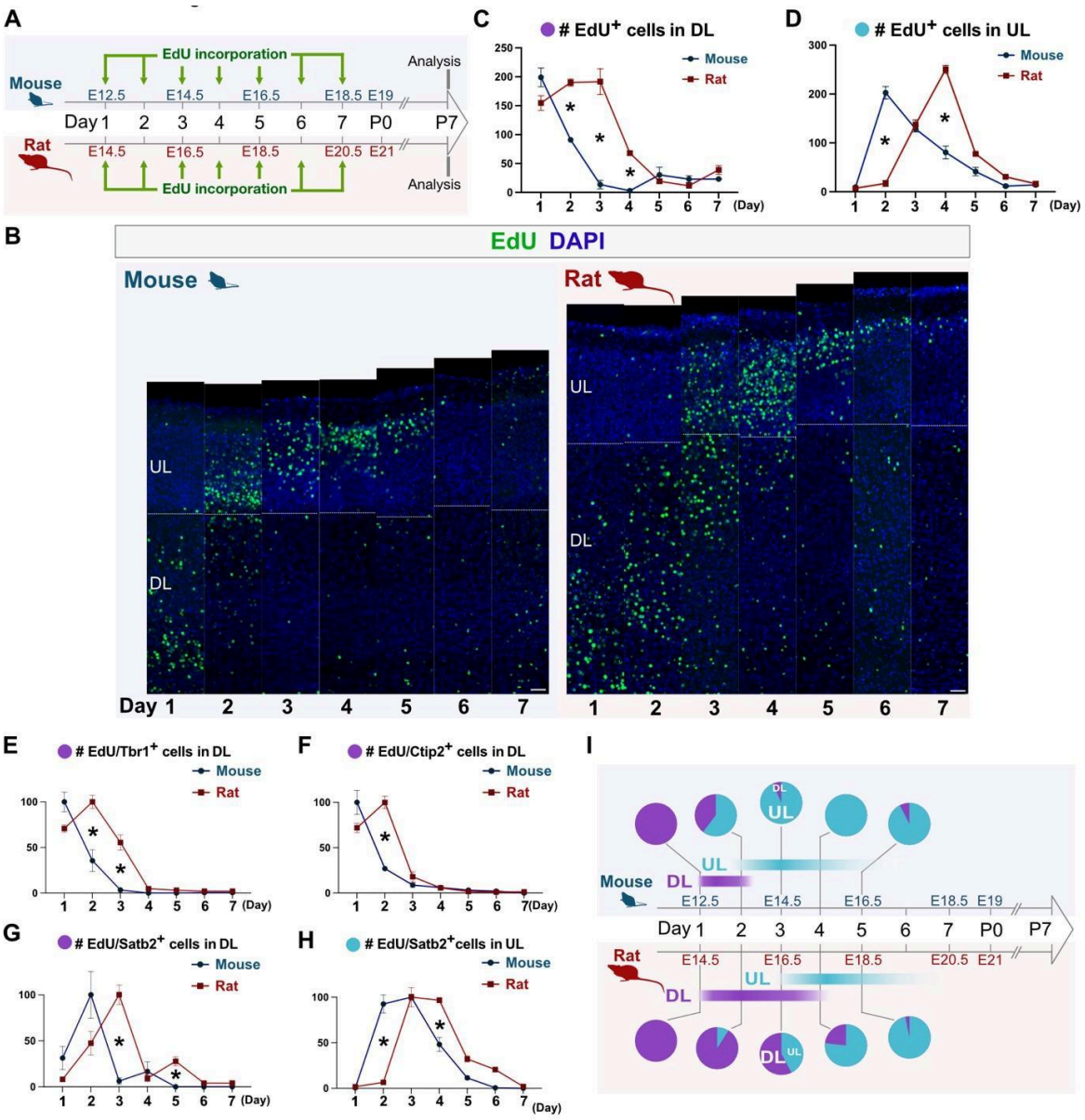

Figure 4. Birthdating of cortical excitatory neurons in mice and rats

(**A**) Experimental design for birthdating analysis in mice and rats, showing different timing of EdU injections from the onset until the end of neurogenesis. (**B**) Representative images of cortical columns in S1 with EdU-labeled neurons at the specified developmental stages. Scale bars: 50 μm. (**C** to **D**). Quantification of DL (C) and UL subtypes (D) labeled with EdU at different stages. Asterisks indicate statistical significance ($p < 0.05$). (**E** to **H**) Normalized counts of neurons colabeled for EdU and projection-specific markers. (E) Tbr1-positive DL neurons, (F) Ctip2-positive DL neurons, (G) Satb2-positive neurons located in DL, and (H) Satb2-positive neurons located in UL. **(I)** Summary of neuronal birthdating in mice and rats, highlighting species-specific differences in the timing of DL and UL neuron production. Statistical analysis was performed using Welch's t-test, with detailed results available in Table S2.

Species-specific timing of DL to UL subtype transition confirmed by axon projection analysis

To further confirm the species-specific timing of the DL to UL subtype switch, characterized by somal location and marker expression (**Fig. 3 and 4**), we examined the axon projection patterns of neurons generated during the mid-neurogenic phase (Days 2.5 and 3). Axonal projections are the defining feature of these subtypes (fig. S5B). We analyzed axon projections of the neurons generated at a certain timing by *in utero* electroporation (IUE) of a plasmid encoding the membrane-anchored fluorescent protein Achilles. This method labeled excitatory neurons in the primary somatosensory cortex and enabled axonal trajectory tracing at P7 (fig. S5A). The laminar distribution of labeled neurons electroporated at Day 2.5 closely matched the results of EdU pulse-labeling at Day 3, which demonstrated the greatest species-specific differences in neuronal composition (fig. S5C). IUE efficiently labeled axons for visualization in whole brains using tissue clearing (fig. S5D) and in slices with immunostaining of Achilles protein with anti-GFP antibody (fig. S5E). In mice, axons of neurons labeled at the mid-neurogenic stage predominantly projected to the corpus callosum. In contrast, in rats, axons from neurons labeled at the same stage projected to both intra- and extra-cortical targets, including the corpus callosum, thalamus, and descending brainstem structures such as the ipsilateral pyramidal tract (fig. S5, D to F). Consistent with previous studies(*17*), neurons generated at Days 1–1.5 in mice projected to brainstem targets, indicating that the DL to UL subtype transition occurs between Days 1.5 and 2 in mice (fig. S5E). These findings align with the birthdating results (**Fig. 3 and 4**), where neurons born at the mid-neurogenic stage (Day 3) in mice were predominantly Satb2-positive UL subtypes in layer 2/3 (CPN). Conversely, in rats, neurons generated at the same stage included more Tbr1-positive CThPN and Ctip2-positive CSPN in layers 5–6. These observations confirm that the mid-neurogenic phase produces distinct neuronal subtypes in mice and rats, defined by axon projection patterns. The differences in axonal targeting reflect the species-specific timing of the DL to UL subtype switch (fig. S5F).

Conservation in neural progenitor cycling and indirect neurogenesis in mice and rats

The species-specific difference in DL neuron production could theoretically arise from transient amplification of neuronal output through either cell cycle acceleration or an increased contribution of intermediate progenitors (IP) via indirect neurogenesis(*18*) during the early DL-producing phase. To explore these possibilities, we analyzed the density of mitotic progenitors in the VZ and subventricular zone (SVZ) of the future primary somatosensory field (**Fig. 5, A to C**). The temporal patterns of mitotic density in both the VZ and SVZ were strikingly conserved between the two species. Additionally, we assessed progenitors in the G2/S phase by administering EdU one hour before sacrifice (**Fig. 5, D and E**). No significant differences were observed in the density of G2/S-phase cells throughout the neurogenic period, except at the end of neurogenesis on Day 7. These findings suggest that cell cycle kinetics, as partly indicated by proportions of progenitors in the M and G2/S phases, are comparable between the two species, consistent with previous studies(*19*, *20*).

Despite the overall conservation, we noted a minor increase in SVZ mitosis in rats compared to mice (**Fig. 5C**). Rats exhibited a relatively higher abundance of IPs in the G2/S phase, co-labeled by EdU and Tbr2, throughout the neurogenic period (**Fig. 5F**). This suggests that indirect neurogenesis plays a more prominent role in rats than in mice, not limited to the early DL production phase but extending across the entire neurogenic period. In conclusion, differences in cell cycle kinetics and indirect neurogenesis are unlikely to be the primary factors driving the species-specific variation in DL neuron production. Instead, the temporal regulation of progenitor neurogenic competence, which determines the duration of the DL production phase, provides a more plausible explanation for the greater number of DL subtypes observed in rats (**Fig. 3 and 4**).

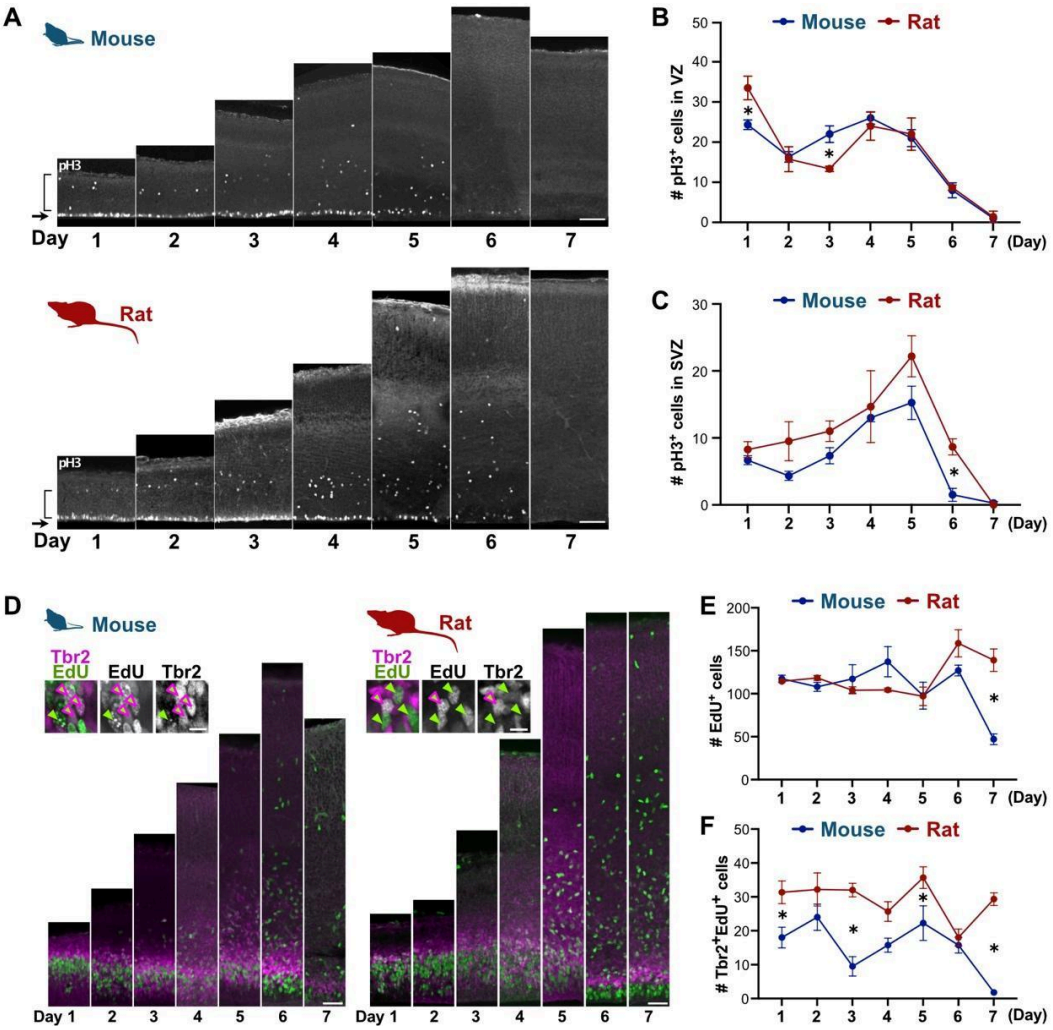

Figure 5. Dynamics of progenitor cell cycle and indirect neurogenesis activity in mouse and rat cortical neurogenesis

(**A** to **C**) Mitotic progenitors in the cortical neurogenesis of mice and rats (Days 1–7) are immunolabeled with phospho-histone H3 antibody. Mitotic RG and IP are

separately quantified in the ventricular zone (VZ, arrows in A; quantification in B) and in the subventricular zone (SVZ, parenthesis in A; quantification in C). (**D**) Cells in the G2/S phase are labeled with EdU administered one hour before sacrifice. (**E**) Total number of EdU-labeled cells during the neurogenic period is quantified. (**F**) Double-labeled EdU and Tbr2-positive cells, identified as IP, are quantified across neurogenic stages. Statistical analysis: Time points with statistically significant differences ($p < 0.05$) are indicated by asterisks (B, C, E, F; Student's t-test).

Non-linear correspondence of temporal progression in cortical RG progenitors in mice and rats revealed by scRNAseq

To investigate the molecular basis of the species-specific temporal dynamics of cortical neurogenesis, we performed comparative scRNAseq analysis of neurogenic progenitors. Using the Chromium X system (10x Genomics), we obtained high-quality transcriptome profiles for 14,290 cells from rat cortices at Days 1 (E14.5), 3 (E16.5), and 5 (E18.5) of neurogenesis (**Fig. 6A**). After quality control, we integrated these profiles with previously published mouse cortical cell data from corresponding neurogenic stages(*21*) (fig. S6). Uniform Manifold Approximation and Projection (UMAP)(*22*) identified 16 distinct cell clusters annotated with commonly used cell type marker genes (**Fig. 6, B and C** and fig. S6, C to E). All major cortical cell types were represented, with no cluster dominated by a single species or developmental stage, indicating clustering was driven by cell type differences rather than species-specific biases or technical artifacts (**Fig. 6, B and D**).

We examined temporal gene expression changes in progenitors, as neuronal laminar fate is determined by the progenitor's developmental age. Using a machine-learning-based ordinal regression model(*23*), we identified stage-specific "progenitor age genes" (Table S3 and fig. S7, A to F), which showed significant overlap between species and with genes identified in previous studies of cortical neurogenesis(*24*, *25*). Gene ontology (GO) analysis revealed enrichment for terms such as "positive regulation of Wnt signaling pathway" in identified progenitor age genes (fig. S7G). To quantitatively compare temporal changes between species, we aligned progenitors by developmental age using a pseudotime analysis based on the expression profiles of progenitor age genes with cellAlign algorism(*26*) (**Fig. 6E**). Corresponding pairs of mouse and rat progenitors were identified by minimizing expression distance. This analysis revealed that most rat progenitors at Day 1 correspond to a smaller subset of mouse progenitors with the youngest pseudotime scores. This indicates that rat progenitors retained early-age expression profiles longer than mouse progenitors, which progressed through developmental aging more rapidly. In contrast, the later neurogenic phase progressed in parallel in both species (Days 1 and 3 in mice and Days 3 and 5 in rats), with exceptions at the end of neurogenesis. Non-linear correspondence in pseudotime changes was observed in more quantitative measurement, with the largest delay in rat progenitors occurring where Day 1 and Day 3 progenitors overlapped (asterisk in **Fig. 6F**). Expression dynamics of individual progenitor age genes supported these trends (**Fig. 6G**). For example, *Cyclin D1 (Ccnd1)*, an early-biased gene, decreased sharply between Days 1 and 3 in mice but remained highly expressed in rats through Days 3 and 5. Similarly, *Fezf2*, which activates the DL determinant *Bcl11b (Ctip2)*(*17*), showed sustained expression in rats compared to mice. Conversely, late-biased genes such as *Pantr1*, *Zbtb20*, and

Fam210b exhibited the opposite pattern. These findings indicate that the molecular program governing the internal developmental age of cortical progenitors progresses more rapidly in mice than in rats, particularly during the early neurogenic phase (**Fig. 6H**). This is in parallel with species-specific generation timings of DL and UL neuron subtypes. In summary, the temporal progression of cortical progenitors exhibits species-specific non-linear scaling, as revealed by single-cell resolution transcriptomics.

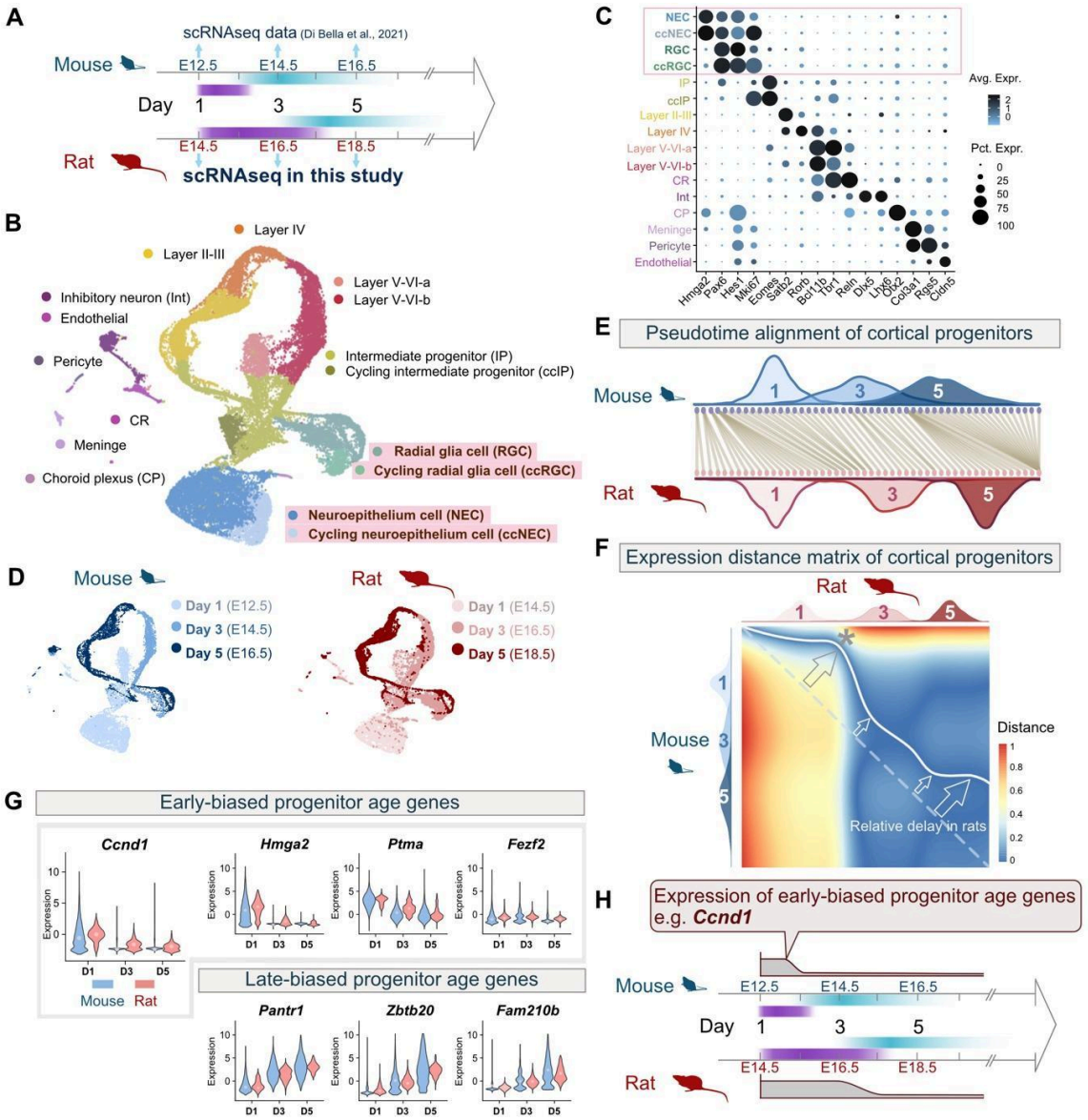

Figure 6. Temporal progression of progenitor aging in the mouse and rat cortical neurogenesis revealed by scRNAseq

(**A**) scRNAseq analysis of rat cortical cells collected at three neurogenic stages (Days 1, 3, and 5) was performed and compared with previously published mouse datasets from corresponding stages. (**B**) UMAP representation of cortical cells from

both species, illustrating the clustering of major cell types. (**C**) Cell type-specific marker genes used for annotation, ensuring consistent identification across species. (**D**) UMAP visualization of cortical cells from three developmental stages in mice and rats. (**E**) Alignment of mouse and rat progenitor cells based on their pseudotime scores. Trajectories in each species were divided into 50 blocks ("Pseudocells") for pairwise distance calculations using dynamic time warping. Histograms display the distribution of cells from sampling stages (Days 1, 3, and 5) along the trajectories. (**F**) Distance matrix of mouse and rat progenitor cells based on "progenitor age gene" expression. Cells were aligned by pseudotime scores along species-specific trajectories. The optimal alignment is indicated by the solid white line, which deviates from the diagonal dotted line, reflecting delayed developmental progression in rats compared to mice. Inflection points (open arrows) highlight significant changes in relative developmental tempo, particularly in the early phase (asterisk). (**G**) Examples of "progenitor age genes" illustrating differences in expression dynamics. Early-biased genes, such as *Ccnd1*, *Hmga2*, and *Ptma*, show a rapid decline in expression between Days 1 and 3 in mice but are more sustained in rats during the same period. (**H**) Schematic representation of the differential expression dynamics of early-biased progenitor age genes, such as *Ccnd1*, in mice and rats, summarizing the temporal progression differences.

Species-specific timing of DL-UL switch is regulated by temporal dynamics of *Ccnd1* expression in RG progenitors

The non-uniformly specified tempo of progenitor aging in mice and rats may contribute to the differential timing of DL-UL switch in cortical neurogenesis, which in turn leads to the differential production of early-born DL neurons. To test this hypothesis, we modulated the temporal progression in rats to mimic that of mice by precociously reducing the expression of early-biased progenitor age genes, focusing on *Ccnd1* (**Fig. 7A**). Among the early-biased progenitor age genes identified, *Ccnd1* was prioritized for its significant enrichment in rats compared to mice during the mid-neurogenic period (Day 3) (**Fig. 6G,** fig. S8, A and B, and Table S4). At this stage, the UL-DL ratio of producing neurons shows the most pronounced species difference (**Fig. 3 and 4**). *Ccnd1* transcription is driven by the canonical Wnt signaling pathway(*27*, *28*), which regulates the temporal progression of cortical progenitors(*29*, *30*). Additionally, previous studies have demonstrated *Ccnd1*'s critical role in the laminar fate of cortical neurons in mice(*31*, *32*).

To suppress *Ccnd1* expression in rat RG progenitors, we introduced short interfering RNA (siRNA) against *Ccnd1* along with a fluorescent marker via *in utero* electroporation (IUE) on Day 2, one day before the onset of significant UL-DL differences. Fluorescent *in situ* hybridization confirmed effective suppression of *Ccnd1* expression in cortical RG progenitors one day after IUE (**Fig. 7B**). The laminar distribution of neurons generated by electroporated progenitors was analyzed at P7 (**Fig. 7, C and D**). Compared to control siRNA, *Ccnd1* siRNA increased the proportion of UL subtypes among labeled neurons. Rescue experiments, co-introducing *Ccnd1* siRNA with human CCND1 cDNA (resistant to siRNA), restored the UL-DL ratio to control levels. Immunohistochemistry further supported these findings, showing that *Ccnd1* knockdown reduced the percentage of Ctip2-positive DL neurons while increasing Satb2-positive UL neurons (**Fig. 7, E to G**). These effects were reversed by the rescue experiment using human CCND1

cDNA. These results demonstrate that sustained *Ccnd1* expression is necessary to maintain the DL-producing progenitor state in rats. Reducing *Ccnd1* expression in the rat mid-neurogenic stage, mimicking the mouse pattern, caused a premature switch from DL to UL subtype production, similar to mouse cortical neurogenesis (**Fig. 7H**). In conclusion, the non-uniformly optimized temporal progression of cortical progenitors in mice and rats, at least partially regulated by the early-biased progenitor age gene *Ccnd1*, contributes to the species-specific DL neuron abundance.

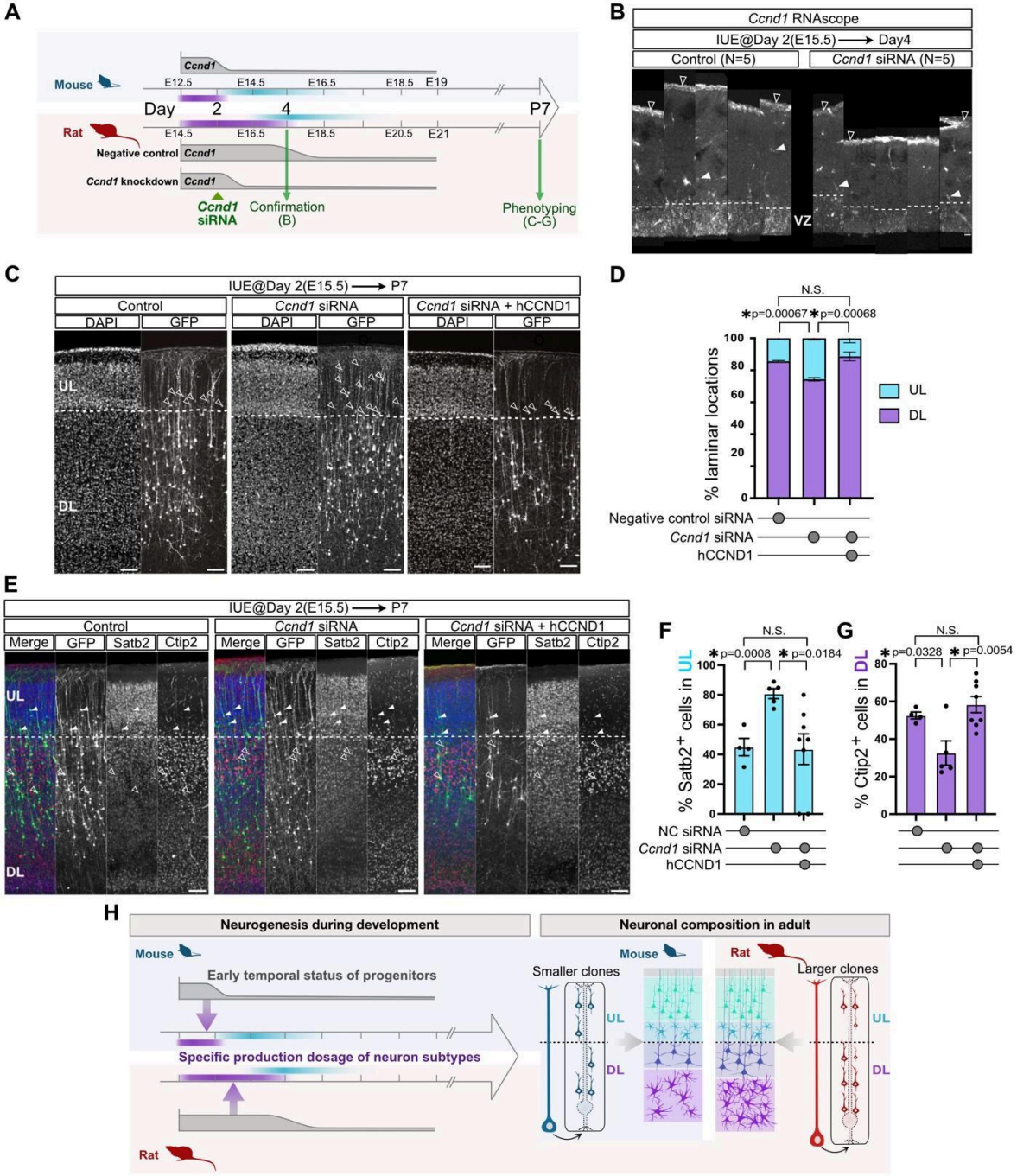

Figure 7. siRNA-mediated knockdown of *Ccnd1* in rat mid-neurogenesis increases UL neurons at the expense of DL neurons

(**A**) Overview of the *Ccnd1* knockdown experiment in rats. siRNA targeting *Ccnd1* was introduced into cortical progenitors via IUE at Day 2 (E15.5). Knockdown efficiency was assessed at Day 3 (E16.5), and the laminar fate of electroporated neurons was examined at P7. (**B**) Knockdown efficiency of *Ccnd1* siRNA was confirmed using fluorescent *in situ* hybridization (RNAscope). Significant reduction in *Ccnd1* signal was observed in the VZ of all five embryos, compared to the control. Signal intensity in vascular (filled arrowheads) and meningeal cells (open arrowheads), which were not targeted by IUE, remained unaffected. (**C**) The laminar distribution of electroporated neurons was analyzed. UL neurons were indicated by open arrowheads. (**D**) Quantification of electroporated neurons in the DL and UL layers demonstrated an increase in UL neurons at the expense of DL neurons following *Ccnd1* knockdown. (**E** to **G**) Marker expression of electroporated neurons was assessed by immunohistochemistry. Satb2-positive UL neurons (filled arrowheads) increased, while Ctip2-positive DL neurons (open arrowheads) decreased after *Ccnd1* knockdown. (**H**) Schematic summary of the study. The sustained expression of *Ccnd1* is necessary to maintain progenitor temporal states in mid-neurogenesis. Reduction of *Ccnd1* mimics the mouse-like temporal progression, resulting in a premature subtype switch from DL to UL neurons. Scale bars: 20 μm (B), 100 μm (C and E), and 10 μm (H).

Discussion

We conducted a comparative analysis of cortical neurogenesis in mice and rats, two closely related rodent species with notable differences in brain size and structure. Histological assessments revealed species-specific variations in cortical excitatory neuron composition: rats exhibit significantly more DL neurons per cortical column than mice, while UL neuron numbers remain comparable between the two species (**Fig. 1**). Clonal analysis demonstrated that rat RG progenitors produce more DL neurons than those in mice, suggesting that different progenitor activity drives species-specific differences in neuron subtype composition (**Fig. 2**). Birthdating assays further indicated an extended phase of DL neurogenesis in rats, followed by a conserved UL generation phase (**Fig. 3 and 4**). Our scRNAseq analysis revealed that rats maintain the early progenitor state associated with DL neuron production for a longer period than mice. This was evidenced by the sustained expression of early-biased progenitor age genes such as *Ccnd1* (**Fig. 6**). Experimental reduction of *Ccnd1* expression in rat RG progenitors via siRNA resulted in precocious UL neuron production, mimicking mouse-like progression (**Fig. 7**). These findings suggest that rats produce more DL neurons by prolonging the early neurogenic state, reflecting a species-specific, non-uniform scaling of an evolutionarily conserved neurogenic program.

Evolutionary adaptations in DL neuron composition

Our study highlights evolutionary adaptations in DL neuron abundance between mice and rats, contrasting with trends in primates where UL neuron numbers have significantly increased. In rats, all examined DL subtypes (Tbr1-, Ctip2-, and

Satb2-expressing neurons) were more abundant than in mice (**Fig. 1**). The increase in Tbr1-expressing CThPN suggests an expansion of corticothalamic projections from layer 6, potentially enhancing cortical feedback to thalamic nuclei and modulating sensory and motor processing(*33*). This raises the question of whether reciprocal thalamocortical connections are also enhanced in rats. Although there is no direct assessment, more prominent thalamic terminals in the rat barrel field support this hypothesis (fig. S1, C and D). The slight increase in Ctip2-expressing CSPN in layer 5 of rats may reflect their larger body size and greater motor control requirements. Although UL neuron numbers were similar between species, Satb2-positive neurons in the DL were more abundant in rats, suggesting enhanced descending outputs from cortico-cortical circuits. Satb2-positive DL neurons uniquely project to both callosal and brainstem targets, compared to UL neurons which project exclusively callosally(*34*, *35*).

Further studies on species-specific DL neuron subtypes could clarify how anatomical differences influence functional and cognitive capabilities. The diversity of DL projection targets is also of interest. Our axon labeling experiments primarily classified projections as intracortical or extracortical (fig. S5). More detailed mapping of DL subtype projection patterns in rats, as has been done in mice(*36*, *37*), could elucidate interspecies differences in extra-cortical projectome. The potential behavioral consequences of varying DL neuron abundance and complexity remain to be explored. While comparative behavioral studies in mice and rats are important, a more precise understanding could be gained from genetically modified mice with specific alterations in DL abundance(*38*). This raises the broader question of whether cortical neuronal composition reflects evolutionary adaptations to distinct ecological niches. Rodent species occupy diverse habitats, and their brain architectures likely facilitate survival in these environments(*39*, *40*). Investigating how specific cortical features enhance evolutionary fitness would provide valuable insights.

Temporal regulation of cortical neurogenesis

The stereotyped temporal sequence of cortical neurogenesis is conserved among mammals and is mediated by molecular program such as canonical Wnt signaling(*29*, *30*). Consistent with previous studies(*23*, *25*), our results confirmed early-biased expression of Wnt-related genes in RG progenitors in both mice and rats. A key downstream mediator of Wnt signaling is *Ccnd1*, whose promoter activity is directly regulated by Wnt-effector Tcf transcription factors in cortical progenitors(*27*, *28*). Although previous studies report some inconsistencies(*41*), *Ccnd1* overexpression alone has been shown to maintain progenitors in a younger temporal state, promoting the production of deeper-layer neuronal fates in mice(*31*, *32*). Similarly, our experiments demonstrated that *Ccnd1* knockdown in rat RG progenitors results in precocious UL neuron generation (**Fig. 7**). These findings suggest that the Wnt-*Ccnd1* molecular axis that regulates the temporal state of cortical progenitors and determines laminar fate of producing neurons is conserved in both species.

Next question is how *Ccnd1* regulates the temporal status of cortical progenitors. *Ccnd1* encodes a D-type cyclin protein that cooperates with cyclin-dependent kinase *Cdk4* to promote the G1/S transition. Higher expression of *Ccnd1* is associated with a

shorter G1 phase duration. Previous studies in mice documented that the G1 phase is shortest at the onset of cortical neurogenesis and elongates progressively as development proceeds(*42*). This pattern correlates with the expression dynamics of *Ccnd1*(*23*, *32*, *43*, *44*). Since G1 represents a critical window when progenitors are responsive to extrinsic signals(*45*), it has been hypothesized that G1 length, which changes in parallel with stage progression, causally influences progenitor behavior(*46*). Overexpressing either *Ccnd1* alone(*41*) or with *Cdk4*(*47*) has been shown to shorten the G1 phase, leading to an increase in proliferative divisions at the expense of neurogenic divisions. This highlights the potential role of G1 duration in progenitor aging. However, we could not detect a significant difference in cell cycle parameters between mice and rats (**Fig. 5**). Moreover, the temporal dynamics of these cell cycle parameters do not correlate with the expression dynamics of *Ccnd1* revealed by scRNAseq (**Fig. 6**). Interestingly, the expression dynamics of *Ccnd1* consistently align with the progenitor aging, as revealed by pseudotime analysis of scRNAseq data (**Fig. 6**), and with the laminar fate of neurons produced in birthdating studies (**Fig. 3 and 4**). Together with previous evidence showing that laminar fate transitions occur even when cell cycle progression is blocked in mice(*48*), our results suggest that the internal temporal state of progenitors regulates the laminar fate of neurons produced but operates independently of cell cycle regulation. This decoupling may offer evolutionary flexibility, allowing independent adaptation of cell cycle kinetics and of neurogenesis dynamics. For example, humans exhibit cortical neurogenesis durations that are an order of magnitude longer than in mice, despite progenitor cell cycle lengths differing by only a few folds(*49–51*). Such flexibility could contribute to species-specific number of neuronal outputs. Beyond its canonical role in G1/S transition with *Cdk4*, *Ccnd1* also functions non-canonically, independent of Cdk proteins(*52*). For example, in retinal development, *Ccnd1* directly binds to the promoters of target genes, such as *Notch1*, in collaboration with epigenetic regulators(*53*). A detailed molecular dissection of *Ccnd1*'s role in cortical neurogenesis, particularly its interaction with temporal regulators such as epigenetic mechanisms(*23*, *54–57*), metabolisms(*11*, *58*, *59*), and membrane potential(*30*), warrants further research.

A crucial question concerns the non-uniform scaling of neurogenetic temporal program in cortical progenitors, as evidenced by the differing *Ccnd1* expression dynamics in mice and rats (**Fig. 6**). Canonical Wnt signaling is a plausible upstream regulator, given that TCF7I1 directly regulates the *Ccnd1* promoter(*27*, *28*). Species-specific temporal dynamics of Wnt ligands from the cortical hem or postmitotic neurons may act as extrinsic regulators of neurogenetic timing(*60*, *61*). Xenograft experiments, such as transplanting rat RG progenitors into the mouse VZ or vice versa, could clarify whether extrinsic control plays a critical regulatory role(*29*, *62*, *63*). Concurrently, cis-regulatory evolution of *Ccnd1* may explain its species-specific expression dynamics. Comparative genomic analysis and chromatin immunoprecipitation using antibodies against potential upstream regulators, such as TCF7I1, could elucidate the mechanisms driving these differences. In summary, investigating both upstream and downstream regulatory factors of *Ccnd1* will deepen our understanding of the non-uniform scaling of temporal progression of cortical progenitors and its contribution to species-specific neuronal compositions.

Evolvability of the mammalian cortical neurogenesis

Our study highlights a distinction between conserved and evolved components of the mammalian neurogenetic program. The early-to-late pattern of cortical neurogenesis is highly conserved across mammals(*1*, *4*, *5*, *64*, *65*) and possibly beyond(*66–68*), suggesting that this developmental process has been maintained due to robust constraints. Despite its apparent rigidity, our comparative analysis of closely related species revealed that subtle adjustments of heterochronic regulation can drive species-specific cortical neuron compositions without fundamentally altering the overall developmental framework. This non-uniform scaling of temporal progression mirrors differences observed in other developmental processes, such as cell differentiation trajectories during gastrulation in mice and rabbits(*69*) and brain development in eutherians and marsupials(*70*). However, it contrasts with the relatively uniform elongation of developmental processes observed in humans compared to mice, as evidenced by studies on cortical neuron maturation(*54*, *71*, *72*), spinal motoneuron generation(*59*), and somitogenesis(*73–75*). Future comparative studies across a broader range of species could help clarify the balance between highly constrained components of the neurogenetic program and its more adaptable elements. Such insights would illuminate how evolutionary diversification optimized cortical architectures for species-specific functional and ecological needs.

Materials and Methods

Animals

All animal procedures were approved by the Institutional Safety Committee on Recombinant DNA Experiments and the Animal Research Committee of the University of Tokyo. ICR mice and WistarST rats were purchased from SLC Japan. Animals were housed in cages with bedding (Avidity Science, TEK-FRESH) and provided constant access to food (Nippon Crea, Rodent Diet CE-2) and water. The animal facility was maintained at a temperature of 23 ± 2°C, a humidity of 50 ± 10%, and a 12-hour light/dark cycle. Plug day was defined as embryonic day (E)0.5, and the day of birth as postnatal day (P)0. Data from all embryos were pooled without discrimination of sex, given the difficulty of determining sex identity at embryonic stages.

Preparation of retroviruses

HEK293T cells were seeded to reach 80–90% confluency on a 10 cm dish. After 24 hours, the cells were transfected with a mixture containing: 0.85 µg pCMV-VSV-G (Addgene #8454), 9.90 µg pUMVC (Addgene #8449), 8.25 µg pRC-2A-EGFP (kind gift from Dr. Pierre Vanderhaeghen and Ryohei Iwata) or pRC-mCherry (prepared in this study). The transfection was performed in 1200 µL of Opti-MEM supplemented with 60 µL of X-tremeGENE. After 24 hours, the medium was replaced, and the cells

were cultured for another 24 hours. The supernatant was then filtered through a 0.45 µm filter, and retroviral particles were concentrated by centrifugation at 25,000 rpm (82,700 g) at 4°C for 2 hours using a 20% sucrose/PBS cushion. The viral pellet was resuspended in 200 µL of cold DPBS, aliquoted in 20 µL, and stored at -80°C. Viral titers were checked using HEK293T cells for each batch.

Retroviral injection to animals *in utero* for clonal tracing

Pregnant females were anesthetized with isoflurane (Viatris, Cat# 114133403), and the uterine horns were exposed under sterile conditions. One microliter of retroviral solution mixed with 1% Fast Green was injected into the fetal lateral ventricles using a heat-pulled capillary. After injection, the uterine horns were returned to the abdominal cavity, and the incisions were sutured. Mice were kept on a heating plate until fully recovered.

***in utero* electroporation**

in utero electroporation was performed with modifications from established protocols(*76*). Timed-pregnant rats (E16.5) or mice were anesthetized with isoflurane. Plasmid solutions (1–1.5 mg/mL DNA) were injected into the embryonic lateral ventricles using heat-pulled capillaries. Electroporation was conducted using tweezer electrodes (Nepa Gene, Cat# CUY650P5) connected to a NEPA21 Type II electroporator (Nepa Gene) with the following settings: Rats: Voltage 50 V, pulse duration 50 ms, interval 950 ms, 4 pulses. Mice: Voltage 50 V, pulse duration 50 ms, interval 950 ms, 6 pulses. Embryos were returned to the abdominal cavity, and the mothers were sutured and placed on a heating plate until recovery. Brains were collected from electroporated pups at P7.

DNA constructs

The coding sequences of rat (NM_171992.6) and human (NM_053056.3) CCND1 were synthesized and subcloned into a CAG promoter-driven expression plasmid (pCAG-IRES-GFP)(*76*) (GenScript Inc.). Membrane-anchored Achilles was amplified by PCR using primers with a membrane targeting signal sequence from the template plasmid (Addgene #153528) and subcloned into a pCAG plasmid. siRNAs for Ccnd1 knockdown were purchased from QIAGEN: Negative control; Cat# 1027310, rat Ccnd1; Cat# SI04717881 and Cat# SI01496222.

Histology and immunostaining

Immunostaining was performed as described previously(*76*). Mouse embryos were collected after electroporation and perfused transcardially with ice-cold 4%

paraformaldehyde (PFA) in PBS. Dissected brains were soaked in 4% PFA overnight at 4°C and sectioned into 100 µm slices using a vibratome (Leica, Cat# VT1000S). Slices were washed with PBST (PBS with 0.1% Triton X-100) three times and incubated in blocking solution (PBS with 0.3% Triton X-100 and 3% donkey serum) for 30 minutes. Brain slices were then incubated overnight at 4°C with primary antibodies (Table S1). After three PBST washes, slices were incubated with secondary antibodies (Table S1) for 2 hours at room temperature. After additional PBST washes, slices were mounted on slide glasses using DAKO glycerol mounting medium (Cat# C0563). Imaging was performed with a confocal microscope (Olympus FV3000), and images were processed using Fiji/ImageJ software(*77*).

Clonal analysis

For clonal analysis, cortical sections were immunostained with anti-GFP and anti-RFP antibodies and imaged sequentially from rostral to caudal using a Slide Scanning Microscope (Keyence, Cat# BZ-X800). Clones were identified as sparse, spatially isolated cell clusters, typically separated by at least 500 µm. Cortical layers (UL vs. DL) were delineated using DAPI staining to define laminar boundaries, and the positions of labeled cells were recorded. Clones were categorized into UL-only, DL-only, or Mixed (UL and DL) types based on the laminar positions of their constituent cells. Clonal lineages with fewer than three cells or more than 30 cells were excluded from quantitative analyses.

Neuronal birthdating

Pregnant animals were injected intraperitoneally with a thymidine analog, 5-ethynyl-2'-deoxyuridine (EdU, Fujifilm; Cat# 052-08843), at 45 mg/kg body weight at designated time points. Brains were collected at P7, and 100 µm coronal sections were prepared using a Vibratome (Leica, Cat# VT1200S). Sections were immunostained with anti-NeuN and anti-Olig2 antibodies to visualize neurons and glial progenitors. EdU incorporation was detected following the Invitrogen EdU detection kit protocol (Click-iT EdU Cell Proliferation Kit, Cat# C10637). EdU-positive cells were counted in cortical sections of 3–4 pups imaged with a confocal microscope (Olympus FV3000).

Tissue clearing and axonal tracing

Tissue clearing was performed using the CUBIC trial kit (Tokyo Chemical Industry Co., Cat# C3942). Fixed samples were washed in PBS for 2 hours (repeated three times) and serially incubated in: 50% CUBIC-L solution for 12 hours at room temperature (RT)100% CUBIC-L solution for 72 hours at 37°C on a shaker. Samples were washed again in PBS for 2 hours (repeated three times), pre-treated in 50% CUBIC-R+ solution for 24 hours at RT on a shaker, and incubated in 100% CUBIC-R+ solution for 24 hours at RT on a shaker. Cleared brains were preserved in

CUBIC-R+, and imaging was conducted with a confocal microscope (Olympus FV3000) in a 3.5 mm dish. Images were processed using Fiji/ImageJ software(*77*).

Single cell transcriptomics

Sample preparation and sequencing

Rat embryonic brains were collected at E14.5, E16.5, and E18.5 and dissociated in ice-cold HBSS (Cat# H6648-500ML, Sigma) containing 0.1% BSA (Cat# 15260-037, Gibco). Tissues were digested in a 25 U/mL papain solution (Cat# 76216-50MG, Sigma) with 55 U/mL DNase (Cat# D4513, Sigma) and 0.5 mM EDTA for 20 minutes. After dissociation and concentration, cells were resuspended in HBSS with 0.04% BSA and processed immediately for single-cell GEM formation, cDNA amplification, and library construction using the Chromium Next GEM Single Cell 3' Kit v3.1 (10x Genomics, PN-1000269) according to the manufacturer's protocol. Libraries were quantified using an Agilent Bioanalyzer and sequenced on the NovaSeq6000 platform (Illumina) with an average read depth of 45,238 (E14.5), 42,669 (E16.5), and 44,504 (E18.5) reads per cell. Sequenced reads were aligned to the rat genome (mRatBN7.2) and processed with CellRanger v6.0.1.

scRNAseq analysis

Downstream analysis was conducted using Seurat v5(*78*). For quality control, cells were filtered using thresholds of nUMI>15000, nGene>15000, log10GenesPerUMI>0.9 and mitoRatio<0.25 to retain high-quality cells. To integrate rat scRNA-seq data with previously published mouse datasets(*21*), we normalized and extracted the 3,000 most variable genes using SCTransform and aligned cells between species with canonical correlation analysis(*79*). PCA dimensionality reduction was performed on integrated data, retaining the first 50 PCs. Cell clustering was conducted using the Louvain algorithm with a resolution of 1.4. Cluster identities were assigned based on the top 50 differentially expressed genes (ranked by -log10 adjusted p-value, Wilcoxon Rank Sum test with Bonferroni correction), ensuring >30% cluster expression and a >0.5 log-fold change threshold, alongside canonical markers (**Fig. 6C**).

Pseudotime age prediction and progenitor age genes

Pseudotime analysis followed established methods(*23*, *80*). L1-regularized ordinal regression was used to predict progenitor cell ages (neuroepithelial and radial glial cells). Analysis was restricted to the 3,000 integration genes to minimize batch effect and sequencing depth variations in the integrated datasets of rat and mouse cells(*21*). We performed the *L1* penalized ordinal regression following the manual from the *psupertime* R package(*80*). After the cross-validation (*n_folds* = 10), the weight of the optimized model was used to rank the genes according to their ability to predict each

progenitor cell age. Genes with non-zero coefficients in both mouse and rat models were classified as "progenitor age genes," reflecting developmental temporal processes (Table 1).

Dynamic time warping-based alignment of pseudotime trajectories in mouse and rat

Dynamic time warping (DTW) of pseudotime trajectories was performed using CellAlign(*26*). Pseudotemporal trajectories for each species were equally spaced into 500 points. Pairwise Euclidean distances between ordered points were calculated using the shared progenitor temporal genes. A fixed-start/fixed-end constraint was applied, identifying the optimal alignment path to minimize overall distance. Gaussian weighting (winSz = 0.1) was applied to reduce noise.

Fluorescent *in situ* hybridization with RNAscope

Rat cortical tissues were cryosectioned at 20 µm thickness using Cryostat (Cat# CM3050S, Leica) and mounted on slide glasses (Cat# MAS-05, Matsunami Glass Ind.,Ltd) following the RNAscope protocol (UM323110, ACDBio). Sections were stored at -80°C until use. Preprocessing, probe hybridization, signal detection, and quantification were performed using the RNAscope Multiplex Fluorescent Detection Kit V2 (Cat# 32310, ACDBio).

Statistical analysis

Statistical analyses were performed using GraphPad Prism 10 (GraphPad Software, Inc., USA) and Microsoft Excel (Microsoft Inc., USA). Experiments were repeated at least three times, and results are expressed as mean ± SEM. Student's t-test: **Fig. 1, B and D, and Fig. 7, D to G**. Welch's t-test: **Fig. 2, E and F, Fig. 3B and Fig. 4, C to H**. Statistical significance thresholds and all quantitative results are summarized in Table S2.

References and notes

1. P. Vanderhaeghen, F. Polleux, Developmental mechanisms underlying the evolution of human cortical circuits. *Nat. Rev. Neurosci.* **24**, 213–232 (2023).

2. A. A. Galakhova, S. Hunt, R. Wilbers, D. B. Heyer, C. P. J. de Kock, H. D. Mansvelder, N. A. Goriounova, Evolution of cortical neurons supporting human cognition. *Trends Cogn. Sci.* **26**, 909–922 (2022).

3. A. R. Desai, S. K. McConnell, Progressive restriction in fate potential by neural progenitors during cerebral cortical development. *Development* **127**, 2863–2872 (2000).

4. D. Jabaudon, Fate and freedom in developing neocortical circuits. *Nat. Commun.* **8** (2017).

5. P. Rakic, Evolution of the neocortex: a perspective from developmental biology. *Nat. Rev. Neurosci.* **10**, 724–735 (2009).

6. I. K. Suzuki, Molecular drivers of human cerebral cortical evolution. *Neurosci. Res.* **151**, 1–14 (2020).

7. Z. Molnár, G. J. Clowry, N. Šestan, A. Alzu'bi, T. Bakken, R. F. Hevner, P. S. Hüppi, I. Kostović, P. Rakic, E. S. Anton, D. Edwards, P. Garcez, A. Hoerder-Suabedissen, A. Kriegstein, New insights into the development of the human cerebral cortex. *J. Anat.* **235**, 432–451 (2019).

8. R. Nehme, O. Pietiläinen, L. E. Barrett, Genomic, molecular, and cellular divergence of the human brain. *Trends Neurosci.* **47**, 491–505 (2024).

9. I. K. Suzuki, P. Vanderhaeghen, Is this a brain which I see before me? Modeling human neural development with pluripotent stem cells. *Development* **142**, 3138–3150 (2015).

10. B. K. Stepien, S. Vaid, W. B. Huttner, Length of the neurogenic period-A key determinant for the generation of upper-layer neurons during neocortex development and evolution. *Front. Cell Dev. Biol.* **9**, 676911 (2021).

11. R. Iwata, P. Vanderhaeghen, Metabolic mechanisms of species-specific developmental tempo. *Dev. Cell* **59**, 1628–1639 (2024).

12. F. Catzeflis, J.-P. Aguilar, J.-J. Jaeger, Muroid rodents: Phylogeny and evolution. *Trends Ecol. Evol.* **7**, 122–126 (1992).

13. C. S. Bresee, H. M. Belli, Y. Luo, M. J. Z. Hartmann, Comparative morphology of the whiskers and faces of mice (Mus musculus) and rats (Rattus norvegicus). *J. Exp. Biol.* **226**, jeb245597 (2023).

14. P. Gao, M. P. Postiglione, T. G. Krieger, L. Hernandez, C. Wang, Z. Han, C. Streicher, E. Papusheva, R. Insolera, K. Chugh, O. Kodish, K. Huang, B. D. Simons, L. Luo, S. Hippenmeyer, S.-H. Shi, Deterministic progenitor behavior and unitary production of neurons in the neocortex. *Cell* **159**, 775–788 (2014).

15. A. Llorca, G. Ciceri, R. Beattie, F. K. Wong, G. Diana, E. Serafeimidou-Pouliou, M. Fernández-Otero, C. Streicher, S. J. Arnold, M. Meyer, S. Hippenmeyer, M. Maravall, O. Marin, A stochastic framework of neurogenesis underlies the assembly of neocortical cytoarchitecture. *Elife* **8** (2019).

16. G. D. Frantz, S. K. McConnell, Restriction of late cerebral cortical progenitors to an upper-layer fate. *Neuron* **17**, 55–61 (1996).

17. L. C. Greig, M. B. Woodworth, M. J. Galazo, H. Padmanabhan, J. D. Macklis, Molecular logic of neocortical projection neuron specification, development and diversity. *Nat. Rev. Neurosci.* **14**, 755–769 (2013).

18. R. F. Hevner, Intermediate progenitors and Tbr2 in cortical development. *J. Anat.* **235**, 616–625 (2019).

19. M. W. Miller, P. E. Kuhn, Cell cycle kinetics in fetal rat cerebral cortex: effects of prenatal treatment with ethanol assessed by a cumulative labeling technique with flow cytometry. *Alcohol. Clin. Exp. Res.* **19**, 233–237 (1995).

20. T. Takahashi, R. S. Nowakowski, V. S. Caviness Jr, The leaving or Q fraction of the murine cerebral proliferative epithelium: a general model of neocortical neuronogenesis. *J. Neurosci.* **16**, 6183–6196 (1996).

21. D. J. Di Bella, E. Habibi, R. R. Stickels, G. Scalia, J. Brown, P. Yadollahpour, S. M. Yang, C. Abbate, T. Biancalani, E. Z. Macosko, F. Chen, A. Regev, P. Arlotta, Molecular logic of cellular diversification in the mouse cerebral cortex. *Nature* **595**, 554–559 (2021).

22. E. Becht, L. McInnes, J. Healy, C.-A. Dutertre, I. W. H. Kwok, L. G. Ng, F. Ginhoux, E. W. Newell, Dimensionality reduction for visualizing single-cell data using UMAP. *Nat. Biotechnol.* **37**, 38–44 (2018).

23. L. Telley, G. Agirman, J. Prados, N. Amberg, S. Fièvre, P. Oberst, G. Bartolini, I. Vitali, C. Cadilhac, S. Hippenmeyer, L. Nguyen, A. Dayer, D. Jabaudon, Temporal patterning of apical progenitors and their daughter neurons in the developing neocortex. *Science* **364** (2019).

24. L. Telley, S. Govindan, J. Prados, I. Stevant, S. Nef, E. Dermitzakis, A. Dayer, D. Jabaudon, Sequential transcriptional waves direct the differentiation of newborn neurons in the mouse neocortex. *Science* **351**, 1443–1446 (2016).

25. T. J. Nowakowski, A. Bhaduri, A. A. Pollen, B. Alvarado, M. A. Mostajo-Radji, E. D. Lullo, M. Haeussler, C. Sandoval-Espinosa, S. J. Liu, D. Velmeshev, J. R. Ounadjela, J. Shuga, X. Wang, D. A. Lim, J. A. West, A. A. Leyrat, W. J. Kent, A. R. Kriegstein, Spatiotemporal gene expression trajectories reveal developmental hierarchies of the human cortex. *Science* **358**, 1318–1323 (2017).

26. A. Alpert, L. S. Moore, T. Dubovik, S. S. Shen-Orr, Alignment of single-cell trajectories to compare cellular expression dynamics. *Nat. Methods* **15**, 267–270 (2018).

27. J. Bonnefont, L. Tiberi, J. van den Ameele, D. Potier, Z. B. Gaber, X. Lin, A. Bilheu, A. Herpoel, F. D. Velez Bravo, F. Guillemot, S. Aerts, P. Vanderhaeghen, Cortical Neurogenesis Requires Bcl6-Mediated Transcriptional Repression of Multiple Self-Renewal-Promoting Extrinsic Pathways. *Neuron* **103**, 1096-1108.e4 (2019).

28. M. Shtutman, J. Zhurinsky, I. Simcha, C. Albanese, M. D'Amico, R. Pestell, A. Ben-Ze'ev, The cyclin D1 gene is a target of the beta-catenin/LEF-1 pathway. *Proc. Natl. Acad. Sci. U. S. A.* **96**, 5522–5527 (1999).

29. P. Oberst, S. Fièvre, N. Baumann, C. Concetti, G. Bartolini, D. Jabaudon, Temporal plasticity of apical progenitors in the developing mouse neocortex. *Nature* **573**, 370–374 (2019).

30. I. Vitali, S. Fièvre, L. Telley, P. Oberst, S. Bariselli, L. Frangeul, N. Baumann, J. J. McMahon, E. Klingler, R. Bocchi, J. Z. Kiss, C. Bellone, D. L. Silver, D. Jabaudon, Progenitor hyperpolarization regulates the sequential generation of neuronal subtypes in the developing neocortex. *Cell* **174**, 1264-1276.e15 (2018).

31. I. Espinosa-Medina, D. Feliciano, C. Belmonte-Mateos, R. Linda Miyares, J. Garcia-Marques, B. Foster, S. Lindo, C. Pujades, M. Koyama, T. Lee, TEMPO enables sequential genetic labeling and manipulation of vertebrate cell lineages. *Neuron* **111**, 345-361.e10 (2023).

32. D. W. Hagey, D. Topcic, N. Kee, F. Reynaud, M. Bergsland, T. Perlmann, J. Muhr, CYCLIN-B1/2 and -D1 act in opposition to coordinate cortical progenitor self-renewal and lineage commitment. *Nat. Commun.* **11**, 2898 (2020).

33. G. M. G. Shepherd, N. Yamawaki, Untangling the cortico-thalamo-cortical loop: cellular pieces of a knotty circuit puzzle. *Nat. Rev. Neurosci.* **22**, 389–406 (2021).

34. E. Sinopoulou, E. S. Rosenzweig, J. M. Conner, D. Gibbs, C. A. Weinholtz, J. L. Weber, J. H. Brock, Y. S. Nout-Lomas, E. Ovruchesky, Y. Takashima, J. S. Biane, H. Kumamaru, L. A. Havton, M. S. Beattie, J. C. Bresnahan, M. H. Tuszynski, Rhesus macaque versus rat divergence in the corticospinal projectome. *Neuron* **110**, 2970-2983.e4 (2022).

35. K. Harb, E. Magrinelli, C. S. Nicolas, N. Lukianets, L. Frangeul, M. Pietri, T. Sun, G. Sandoz, F. Grammont, D. Jabaudon, M. Studer, C. Alfano, Area-specific development of distinct projection neuron subclasses is regulated by postnatal epigenetic modifications. *Elife* **5**, e09531 (2016).

36. L. Gao, S. Liu, L. Gou, Y. Hu, Y. Liu, L. Deng, D. Ma, H. Wang, Q. Yang, Z. Chen, D. Liu, S. Qiu, X. Wang, D. Wang, X. Wang, B. Ren, Q. Liu, T. Chen, X. Shi, H. Yao, C. Xu, C. T. Li, Y. Sun, A. Li, Q. Luo, H. Gong, N. Xu, J. Yan, Single-neuron projectome of mouse prefrontal cortex. *Nat. Neurosci.* **25**, 515–529 (2022).

37. R. Muñoz-Castañeda, B. Zingg, K. S. Matho, X. Chen, Q. Wang, N. N. Foster, A. Li, A. Narasimhan, K. E. Hirokawa, B. Huo, S. Bannerjee, L. Korobkova, C. S. Park, Y.-G. Park, M. S. Bienkowski, U. Chon, D. W. Wheeler, X. Li, Y. Wang, M. Naeemi, P. Xie, L. Liu, K. Kelly, X. An, S. M. Attili, I. Bowman, A. Bludova, A. Cetin, L. Ding, R. Drewes, F. D'Orazi, C. Elowsky, S. Fischer, W. Galbavy, L. Gao, J. Gillis, P. A. Groblewski, L. Gou, J. D. Hahn, J. T. Hatfield, H. Hintiryan, J. J. Huang, H. Kondo, X. Kuang, P. Lesnar, X. Li, Y. Li, M. Lin, D. Lo, J. Mizrachi, S. Mok, P. R. Nicovich, R. Palaniswamy, J. Palmer, X. Qi, E. Shen, Y.-C. Sun, H. W. Tao, W. Wakemen, Y. Wang, S. Yao, J. Yuan, H. Zhan, M. Zhu, L. Ng, L. I. Zhang, B. K. Lim, M. Hawrylycz, H. Gong, J. C. Gee, Y. Kim, K. Chung, X. W. Yang, H. Peng, Q. Luo, P. P. Mitra, A. M. Zador, H. Zeng, G. A. Ascoli, Z. Josh Huang, P. Osten, J. A. Harris, H.-W. Dong, Cellular anatomy of the mouse primary motor cortex. *Nature* **598**, 159–166 (2021).

38. W. Zhang, L. Ma, M. Yang, Q. Shao, J. Xu, Z. Lu, Z. Zhao, R. Chen, Y. Chai, J.-F. Chen, Cerebral organoid and mouse models reveal a RAB39b-PI3K-mTOR pathway-dependent dysregulation of cortical development leading to macrocephaly/autism phenotypes. *Genes Dev.* **34**, 580–597 (2020).

39. L. D. Verde Arregoitia, D. O. Fisher, M. Schweizer, Morphology captures diet and locomotor types in rodents. *R. Soc. open sci.* **4**, 160957 (2017).

40. L. D. Verde Arregoitia, G. D'Elía, Classifying rodent diets for comparative research. *Mamm. Rev.* **51**, 51–65 (2021).

41. L.-J. Pilaz, D. Patti, G. Marcy, E. Ollier, S. Pfister, R. J. Douglas, M. Betizeau, E. Gautier, V. Cortay, N. Doerflinger, H. Kennedy, C. Dehay, Forced G1-phase reduction alters mode of division, neuron number, and laminar phenotype in the cerebral cortex. *Proc. Natl. Acad. Sci. U. S. A.* **106**, 21924–21929 (2009).

42. T. Takahashi, R. S. Nowakowski, V. S. Caviness Jr, The cell cycle of the pseudostratified ventricular epithelium of the embryonic murine cerebral wall. *J. Neurosci.* **15**, 6046–6057 (1995).

43. N. Micali, S. Ma, M. Li, S.-K. Kim, X. Mato-Blanco, S. K. Sindhu, J. I. Arellano, T. Gao, M. Shibata, K. T. Gobeske, A. Duque, G. Santpere, N. Sestan, P. Rakic, Molecular programs of regional specification and neural stem cell fate progression in macaque telencephalon. *Science* **382**, eadf3786 (2023).

44. E. Braun, M. Danan-Gotthold, L. E. Borm, K. W. Lee, E. Vinsland, P. Lönnerberg, L. Hu, X. Li, X. He, Ž. Andrusivová, J. Lundeberg, R. A. Barker, E. Arenas, E. Sundström, S. Linnarsson, Comprehensive cell atlas of the first-trimester developing human brain. *Science* **382**, eadf1226 (2023).

45. S. Dalton, Linking the cell cycle to cell fate decisions. *Trends Cell Biol.* **25**, 592–600 (2015).

46. C. Dehay, H. Kennedy, Cell-cycle control and cortical development. *Nat. Rev. Neurosci.* **8**, 438–450 (2007).

47. C. Lange, W. B. Huttner, F. Calegari, Cdk4/cyclinD1 overexpression in neural stem cells shortens G1, delays neurogenesis, and promotes the generation and expansion of basal progenitors. *Cell Stem Cell* **5**, 320–331 (2009).

48. M. Okamoto, T. Miyata, D. Konno, H. R. Ueda, T. Kasukawa, M. Hashimoto, F. Matsuzaki, A. Kawaguchi, Cell-cycle-independent transitions in temporal identity of mammalian neural progenitor cells. *Nat. Commun.* **7**, 11349 (2016).

49. P. Salomoni, F. Calegari, Cell cycle control of mammalian neural stem cells: putting a speed limit on G1. *Trends Cell Biol.* **20**, 233–243 (2010).

50. A. I. Lukaszewicz, D. J. Anderson, Cyclin D1 promotes neurogenesis in the developing spinal cord in a cell cycle-independent manner. *Proc. Natl. Acad. Sci. U. S. A.* **108**, 11632–11637 (2011).

51. D. R. Kornack, P. Rakic, Changes in cell-cycle kinetics during the development and evolution of primate neocortex. *Proc. Natl. Acad. Sci. U. S. A.* **95**, 1242–1246 (1998).

52. P. Hydbring, M. Malumbres, P. Sicinski, Non-canonical functions of cell cycle cyclins and cyclin-dependent kinases. *Nat. Rev. Mol. Cell Biol.* **17**, 280–292 (2016).

53. F. Bienvenu, S. Jirawatnotai, J. E. Elias, C. A. Meyer, K. Mizeracka, A. Marson, G. M. Frampton, M. F. Cole, D. T. Odom, J. Odajima, Y. Geng, A. Zagozdzon, M. Jecrois, R. A. Young, X. S. Liu, C. L. Cepko, S. P. Gygi, P. Sicinski, Transcriptional role of cyclin D1 in development revealed by a genetic-proteomic screen. *Nature* **463**, 374–378 (2010).

54. G. Ciceri, A. Baggiolini, H. S. Cho, M. Kshirsagar, S. Benito-Kwiecinski, R. M. Walsh, K. A. Aromolaran, A. J. Gonzalez-Hernandez, H. Munguba, S. Y. Koo, N. Xu, K. J. Sevilla, P. A. Goldstein, J. Levitz, C. S. Leslie, R. P. Koche, L. Studer, An epigenetic barrier sets the timing of human neuronal maturation. *Nature* **626**, 881–890 (2024).

55. Q. Wu, Y. Shichino, T. Abe, T. Suetsugu, A. Omori, H. Kiyonari, S. Iwasaki, F. Matsuzaki, Selective translation of epigenetic modifiers affects the temporal pattern and differentiation of neural stem cells. *Nat. Commun.* **13**, 470 (2022).

56. Y. Kishi, Y. Fujii, Y. Hirabayashi, Y. Gotoh, HMGA regulates the global chromatin state and neurogenic potential in neocortical precursor cells. *Nat. Neurosci.* **15**, 1127–1133 (2012).

57. Y. Hirabayashi, Y. Gotoh, Epigenetic control of neural precursor cell fate during development. *Nat. Rev. Neurosci.* **11**, 377–388 (2010).

58. R. Iwata, P. Casimir, P. Vanderhaeghen, Mitochondrial dynamics in postmitotic cells regulate neurogenesis. *Science* **369**, 858–862 (2020).

59. T. Rayon, D. Stamataki, R. Perez-Carrasco, L. Garcia-Perez, C. Barrington, M. Melchionda, K. Exelby, J. Lazaro, V. L. J. Tybulewicz, E. M. C. Fisher, J. Briscoe, Species-specific pace of development is associated with differences in protein stability. *Science* **369**, eaba7667 (2020).

60. G. Caronia-Brown, M. Yoshida, F. Gulden, S. Assimacopoulos, E. A. Grove, The cortical hem regulates the size and patterning of neocortex. *Development* **141**, 2855–2865 (2014).

61. E. A. Grove, S. Tole, J. Limon, L.-W. Yip, C. W. Ragsdale, The hem of the embryonic cerebral cortex is defined by the expression of multiple Wnt genes and is compromised in Gli3-deficient mice. *Development* **125**, 2315–2325 (1998).

62. F. Nagashima, I. K. Suzuki, A. Shitamukai, H. Sakaguchi, M. Iwashita, T. Kobayashi, S. Tone, K. Toida, P. Vanderhaeghen, Y. Kosodo, Novel and robust transplantation reveals the acquisition of polarized processes by cortical cells derived from mouse and human pluripotent stem cells. *Stem Cells Dev.* **23**, 2129–2142 (2014).

63. S. K. McConnell, Fates of visual cortical neurons in the ferret after isochronic and heterochronic transplantation. *J. Neurosci.* **8**, 945–974 (1988).

64. J. H. Lui, D. V. Hansen, A. R. Kriegstein, Development and evolution of the human neocortex. *Cell* **146**, 18–36 (2011).

65. E. Taverna, M. Götz, W. B. Huttner, The cell biology of neurogenesis: toward an understanding of the development and evolution of the neocortex. *Annu. Rev. Cell Dev. Biol.* **30**, 465–502 (2014).

66. I. K. Suzuki, T. Kawasaki, T. Gojobori, T. Hirata, The temporal sequence of the mammalian neocortical neurogenetic program drives mediolateral pattern in the chick pallium. *Dev. Cell* **22**, 863–870 (2012).

67. I. K. Suzuki, T. Hirata, Neocortical neurogenesis is not really "neo": a new evolutionary model derived from a comparative study of chick pallial development. *Dev. Growth Differ.* **55**, 173–187 (2013).

68. G. Furlan, V. Cuccioli, N. Vuillemin, L. Dirian, A. J. Muntasell, M. Coolen, N. Dray, S. Bedu, C. Houart, E. Beaurepaire, I. Foucher, L. Bally-Cuif, Life-Long Neurogenic Activity of Individual Neural Stem Cells and Continuous Growth Establish an Outside-In Architecture in the Teleost Pallium. *Current Biology* **27**, 3288-3301.e3 (2017).

69. Y. Mayshar, O. Raz, S. Cheng, R. Ben-Yair, R. Hadas, N. Reines, M. Mittnenzweig, O. Ben-Kiki, A. Lifshitz, A. Tanay, Y. Stelzer, Time-aligned hourglass gastrulation models in rabbit and mouse. *Cell* **186**, 2610-2627.e18 (2023).

70. A. Paolino, E. H. Haines, E. J. Bailey, D. A. Black, C. Moey, F. García-Moreno, L. J. Richards, R. Suárez, L. R. Fenlon, Non-uniform temporal scaling of developmental processes in the mammalian cortex. *Nat. Commun.* **14**, 5950 (2023).

71. R. Iwata, P. Casimir, E. Erkol, L. Boubakar, M. Planque, I. M. Gallego López, M. Ditkowska, V. Gaspariunaite, S. Beckers, D. Remans, K. Vints, A. Vandekeere, S. Poovathingal, M. Bird, I. Vlaeminck, E. Creemers, K. Wierda, N. Corthout, P. Vermeersch, S. Carpentier, K. Davie, M. Mazzone, N. V. Gounko, S. Aerts, B. Ghesquière, S.-M. Fendt, P. Vanderhaeghen, Mitochondria metabolism sets the species-specific tempo of neuronal development. *Science* **379**, eabn4705 (2023).

72. C. Charrier, K. Joshi, J. Coutinho-Budd, J.-E. Kim, N. Lambert, J. de Marchena, W.-L. Jin, P. Vanderhaeghen, A. Ghosh, T. Sassa, F. Polleux, Inhibition of SRGAP2 function by its human-specific paralogs induces neoteny during spine maturation. *Cell* **149**, 923–935 (2012).

73. M. Matsuda, H. Hayashi, J. Garcia-Ojalvo, K. Yoshioka-Kobayashi, R. Kageyama, Y. Yamanaka, M. Ikeya, J. Toguchida, C. Alev, M. Ebisuya, Species-specific segmentation clock periods are due to differential biochemical reaction speeds. *Science* **369**, 1450–1455 (2020).

74. J. Lázaro, M. Costanzo, M. Sanaki-Matsumiya, C. Girardot, M. Hayashi, K. Hayashi, S. Diecke, T. B. Hildebrandt, G. Lazzari, J. Wu, S. Petkov, R. Behr, V. Trivedi, M. Matsuda, M. Ebisuya, A stem cell zoo uncovers intracellular scaling of developmental tempo across mammals. *Cell Stem Cell* **30**, 938-949.e7 (2023).

75. M. Diaz-Cuadros, T. P. Miettinen, O. S. Skinner, D. Sheedy, C. M. Díaz-García, S. Gapon, A. Hubaud, G. Yellen, S. R. Manalis, W. M. Oldham, O. Pourquié, Metabolic regulation of species-specific developmental rates. *Nature* **613**, 550–557 (2023).

76. I. K. Suzuki, D. Gacquer, R. Van Heurck, D. Kumar, M. Wojno, A. Bilheu, A. Herpoel, N. Lambert, J. Cheron, F. Polleux, V. Detours, P. Vanderhaeghen, Human-Specific

NOTCH2NL Genes Expand Cortical Neurogenesis through Delta/Notch Regulation. *Cell* **173**, 1370-1384.e16 (2018).

77. J. Schindelin, C. T. Rueden, M. C. Hiner, K. W. Eliceiri, The ImageJ ecosystem: An open platform for biomedical image analysis. *Mol. Reprod. Dev.* **82**, 518–529 (2015).

78. R. Satija, J. A. Farrell, D. Gennert, A. F. Schier, A. Regev, Spatial reconstruction of single-cell gene expression data. *Nat. Biotechnol.* **33**, 495–502 (2015).

79. T. Stuart, A. Butler, P. Hoffman, C. Hafemeister, E. Papalexi, W. M. Mauck 3rd, Y. Hao, M. Stoeckius, P. Smibert, R. Satija, Comprehensive integration of single-cell data. *Cell* **177**, 1888-1902.e21 (2019).

80. W. Macnair, R. Gupta, M. Claassen, psupertime: supervised pseudotime analysis for time-series single-cell RNA-seq data. *Bioinformatics* **38**, i290–i298 (2022).

Acknowledgments

We are grateful to our colleagues in the lab and common laboratory facilities in the WINGS-LST graduate program the Univerisy of Tokyo. We thank Mr. Naoto Ohte, Drs. Ryohei Iwata, Noruhiko Yamamoto, Tatsumi Hirata, Tadashi Nomura, Kaoru Sugimura, and Carina Hanashima for insightful suggestions for the project and the manuscript. Computations were partially performed on the NIG supercomputer at ROIS National Institute of Genetics.

Funding:
Japan Agency for Medical Research and Development, Research Support Project for Life Science and Drug Discovery (Basis for Supporting Innovative Drug Discovery and Life Science Research (BINDS)) Grant Number JP24ama121020 (MB, YK)
National Institute of Genetics supercomputer (IKS)
Japan Society for the Promotion of Science Grants-in-Aid for Scientific Research (KAKENHI) PAGS Grant Number JP22H04925 (IKS)
Japan Agency for Medical Research and Development, PRIME Understanding of the biological phenomena and responses at the early life stages to improve the quality of health and medical care Grant Number JP20gm6310006 (IKS)
Japan Agency for Medical Research and Development Program for Promoting Platform of Genomics based Drug Discovery Grant Number 24tm0524007 (IKS)
Japan Science and Technology Agency Fusion Oriented REsearch for disruptive Science and Technology program Grant Number JPMJFR214T (IKS)
Japan Society for the Promotion of Science Grants-in-Aid for Scientific Research (KAKENHI) Grant Number JP22H02628 (IKS)
Japan Society for the Promotion of Science Grants-in-Aid for Scientific Research (KAKENHI) Grant Number JP20H04860 (IKS)
Molecular Biology Society of Japan Tomizawa Jun-ichi & Keiko Fund of Molecular Biology Society of Japan for Young Scientist (IKS)
Takeda Science Foundation Life Science Research Grant (IKS)
SECOM Science and Technology Foundation (IKS)

Japan Science and Technology Agency The University of Tokyo Support for Pioneering Research Initiated by Next Generation SPRING GX (YY)
The University of Tokyo World-leading Innovative Graduate Study Program WINGS-LST (XDZ)

Author contributions:
Conceptualization: IKS, YY, XDZ
Methodology: IKS, YY, TR, XDZ, PR, SD, TN, MB, YK
Investigation: IKS, YY, TR, XDZ, PR,
Supervision: IKS, KE
Writing-original draft: IKS, YY, XDZ
Writing-review & editing: IKS, YY, YK, XDZ

Competing interests: The authors declare no competing interests.

Data and materials availability: All animals and reagents generated in this study are available from the lead contact with a completed Materials Transfer Agreement. All data and the codes for analyzing the data in this study are available from the lead contact. Single cell RNA sequencing data of rat cortical cells are available in NCBI Gene Expression Omnibus (GEO: GSE287210).

Supplementary Materials

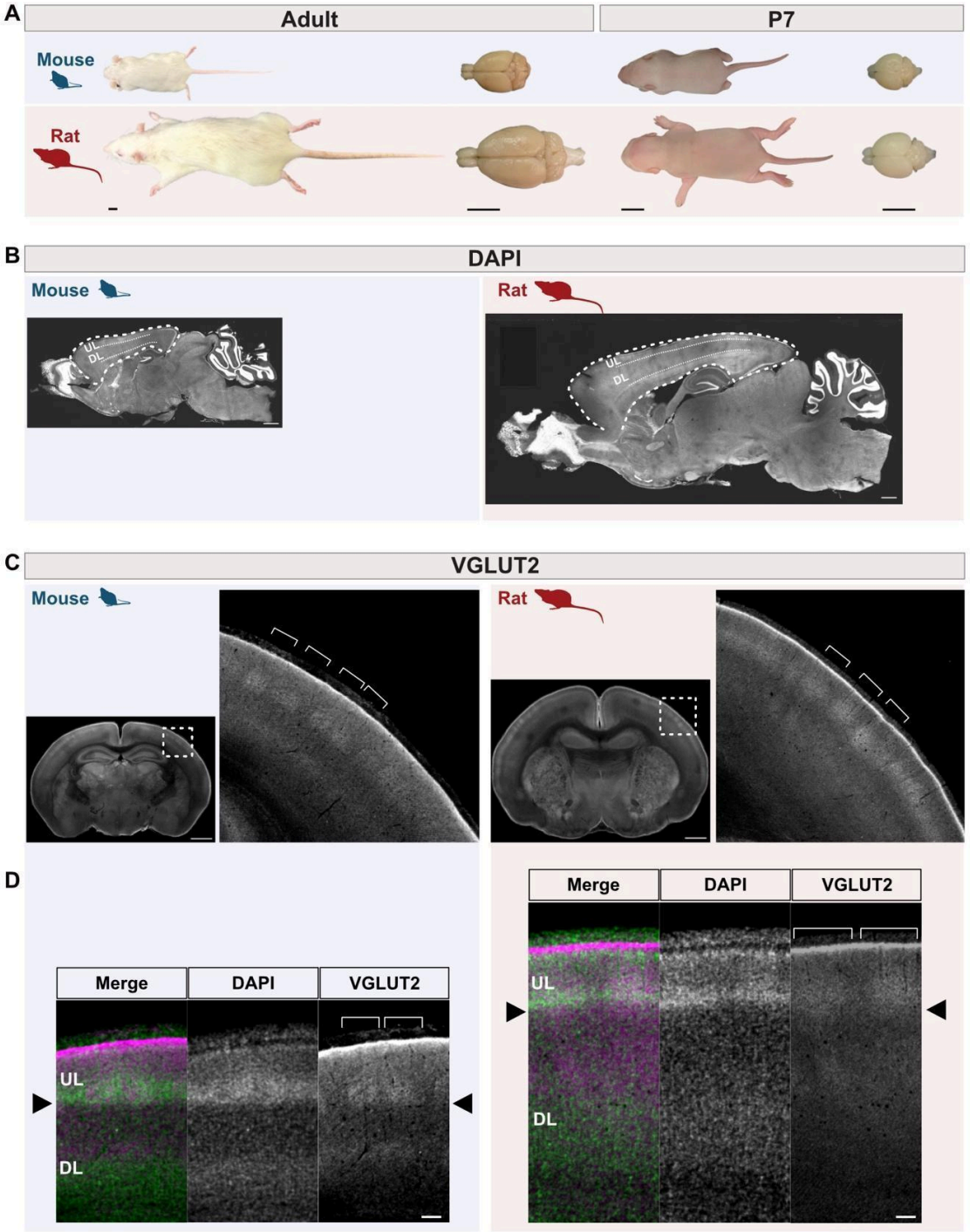

Supplementary Figure S1. Morphological and histological comparison of mouse and rat cerebral cortices

(**A**) Whole-body and brain size differences between mice and rats. (**B**) Sagittal sections of mouse and rat brains at identical magnification. (**C**) Analyses were conducted in the primary somatosensory field (S1) of both species, identified by the characteristic barrel structure of thalamic axon terminals visualized by VGLUT2 immunostaining. Magnified images highlight the structure within dotted rectangles. (**D**) The border between UL (layer 2-4) and DL (layer 5 and 6) is defined by differences in cell density (DAPI staining) and the lower limit of

VGLUT2-positive thalamic fibers (arrowheads). Scale bars: 1 cm (A), 1 mm (B), 1 mm (C), 100 μm (D).

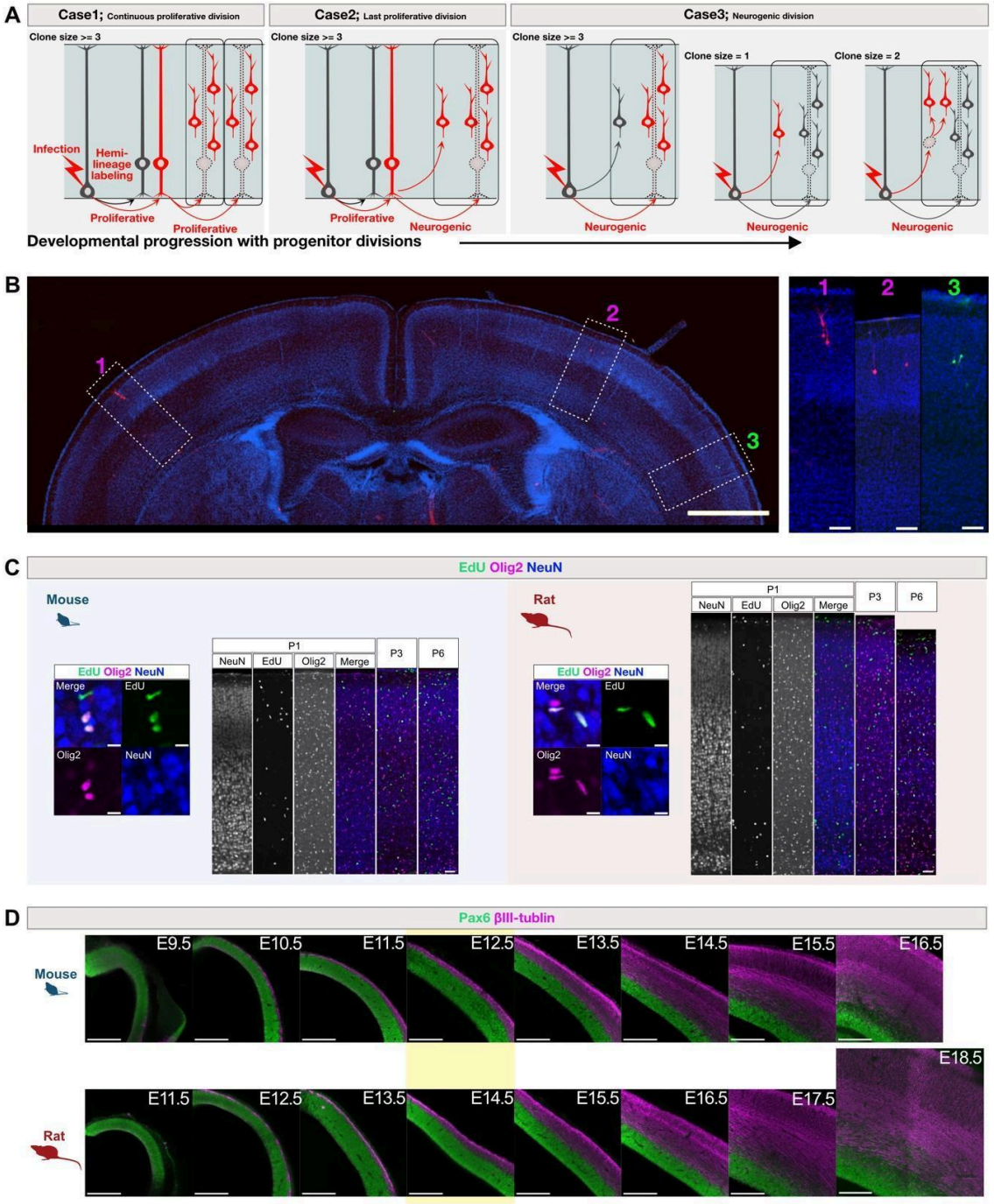

Supplementary Figure S2. Clonal analysis of cortical RG progenitors in mice and rats from the onset to the end of excitatory neurogenesis

(**A**) Schematic representation of hemi-lineage labeling via retroviral gene transfer, illustrating three scenarios of progenitor labeling. A "clonal unit" of neurons is defined as sister excitatory neurons that share a common progenitor origin and are produced during the first and subsequent neurogenic divisions of the mother progenitor (rounded boxes). Case 1: The retroviral vector infects a progenitor undergoing consecutive symmetric proliferative divisions. Case 2: The retroviral vector infects a progenitor at its last proliferative division before initiating neurogenesis. This is the ideal case to label and distinguish the entire clonal unit of sister neurons. Case 3: The retroviral vector infects a progenitor that has already started neurogenic divisions, which will result in only one neuron (direct neurogenesis) or

two neurons (indirect neurogenesis via intermediate progenitors) be labeled. (**B**) Representative coronal section showing three labeled clones (RFP in magenta, GFP in green) with spatial separation and no overlap. (**C**) EdU labeling of postnatal (P1, P3, P6) mice and rats reveals co-labeling with Olig2 (glial progenitors) but not NeuN (neurons), suggesting no neurogenesis in the postnatal period in both species. (**D**) Neuron-progenitor ratio defined by Pax6 (green) and beta III tubulin (magenta) expression demonstrates developmental stage correspondence between species with a two-day difference. E12.5 in mice and E14.5 in rats are the corresponding timing of onset of neurogenesis for the majority of cortical progenitors (yellow background). Scale bars: 1 mm (low magnification, B), 100 µm (magnified images, B), 50 µm (C), 200 µm (D).

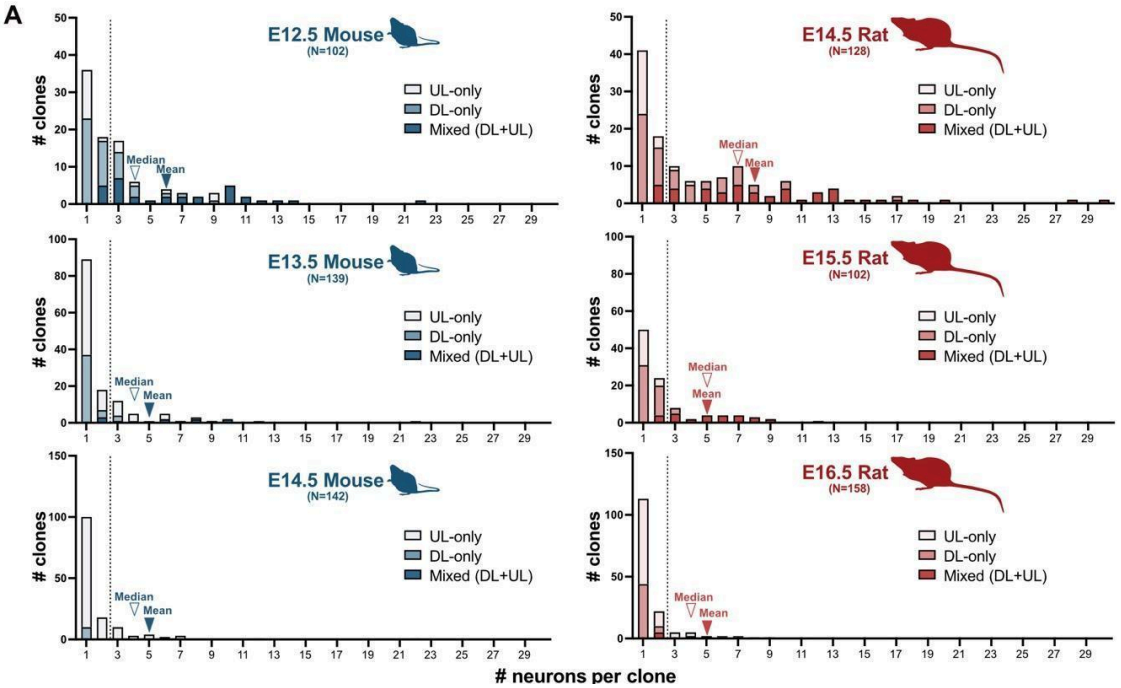

Supplementary Figure S3. Clonal analysis with different retroviral injection timings (**A to F**). Distribution of clonal sizes in mice and rats with retroviral injections at different stages. Clone categories are visualized using color intensity.

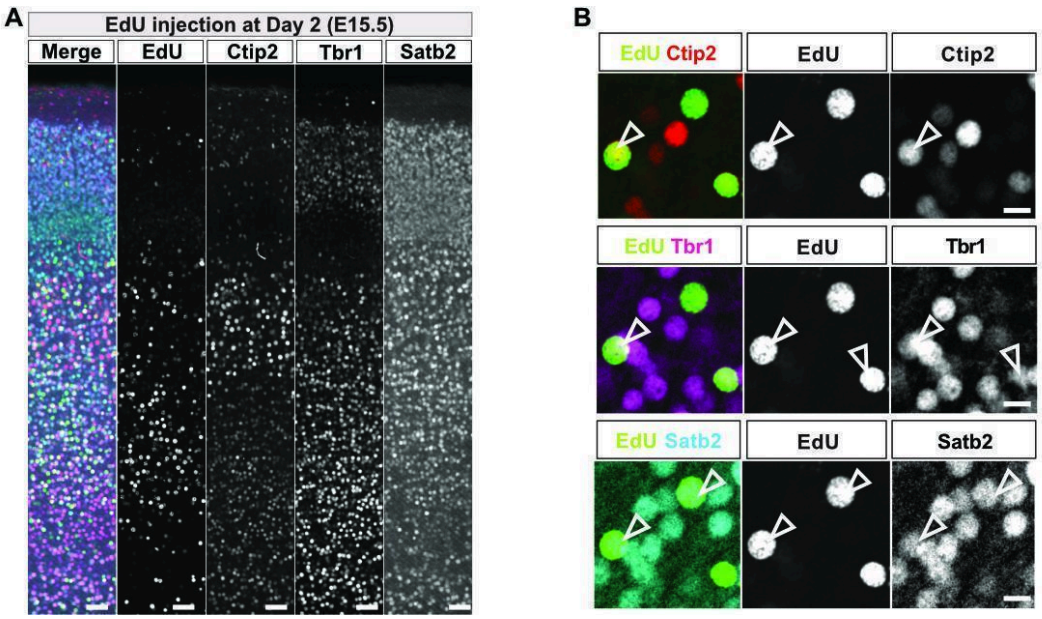

Supplementary Figure S4. Marker immunoreactivility of EdU-labeled neurons.
(**A and B**) Representative images of cortical neurons co-labeled with EdU and subtype-specific markers. Open arrowheads indicate double-positive cells. Scale bars: 50μm (A), 10 μm (B).

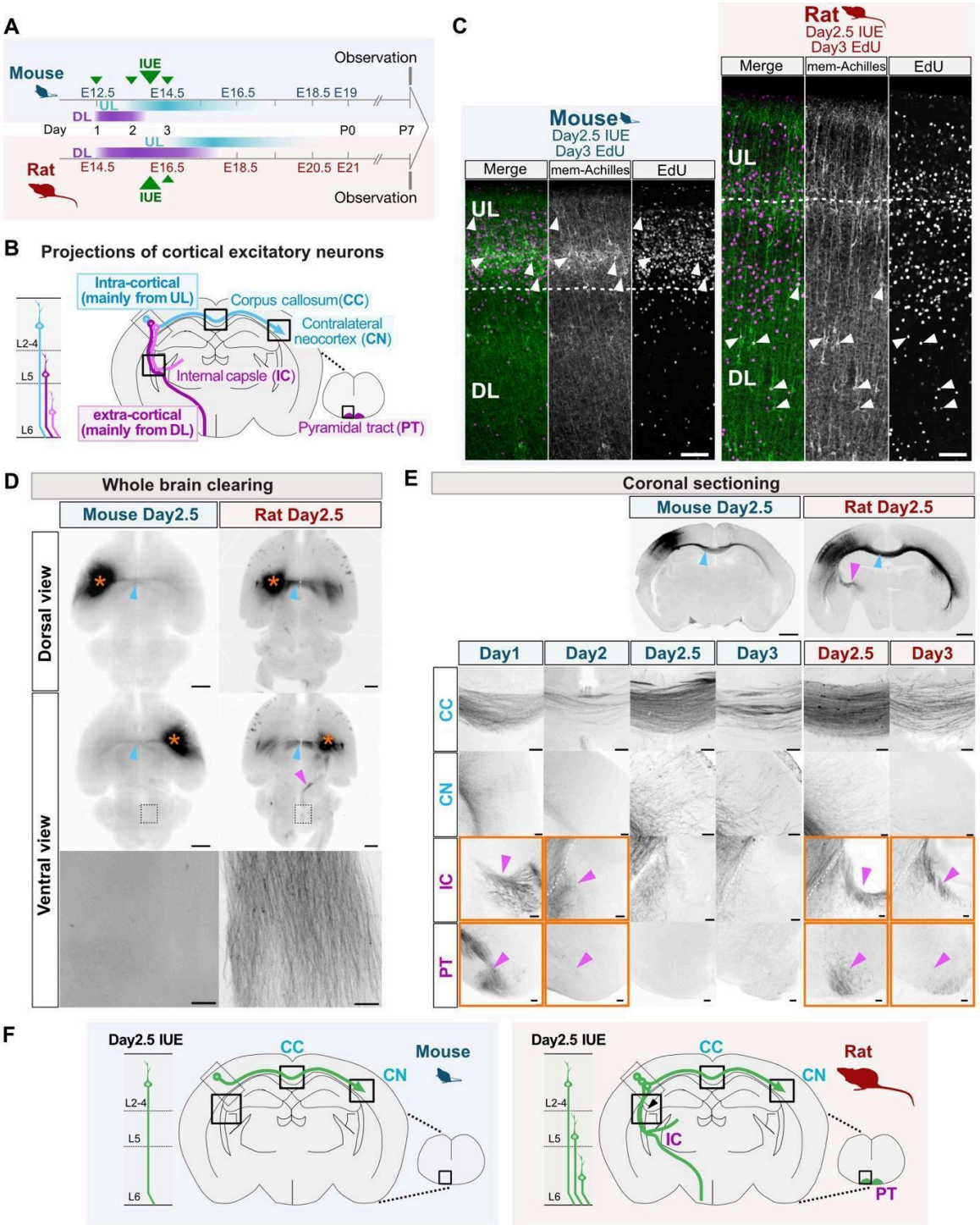

Supplementary Figure S5. Projection identity of neurons generated at Day 2.5-3 of neurogenesis in mice and rats by *in utero* electroporation of a membrane anchored fluorescent protein

(**A**) Schematic of IUE timing and sacrifice for axon projection analysis. (**B**) Major projection targets of cortical excitatory neurons: corpus callosum (CC), contralateral neocortex (CN), internal capsule (IC), and pyramidal tract (PT). (**C**) The neurons electroporated at Day 2.5 are co-labeled with EdU injected at Day 3 in both species. (**D**) Tissue-cleared whole-brain images (dorsal and ventral views) show distinct projection patterns. In rats, prominent ipsilateral projections to the brainstem (magenta arrowheads) are unique. (**E**) Coronal sections confirm unique descending projections in rats and their absence in mice after Day 3

IUE. (**F**) Summary illustration of projection differences between mouse and rat neurons generated at Days 2.5–3. Scale bars: 1 mm (low magnification, C to E), 100 μm (magnified images, D to E).

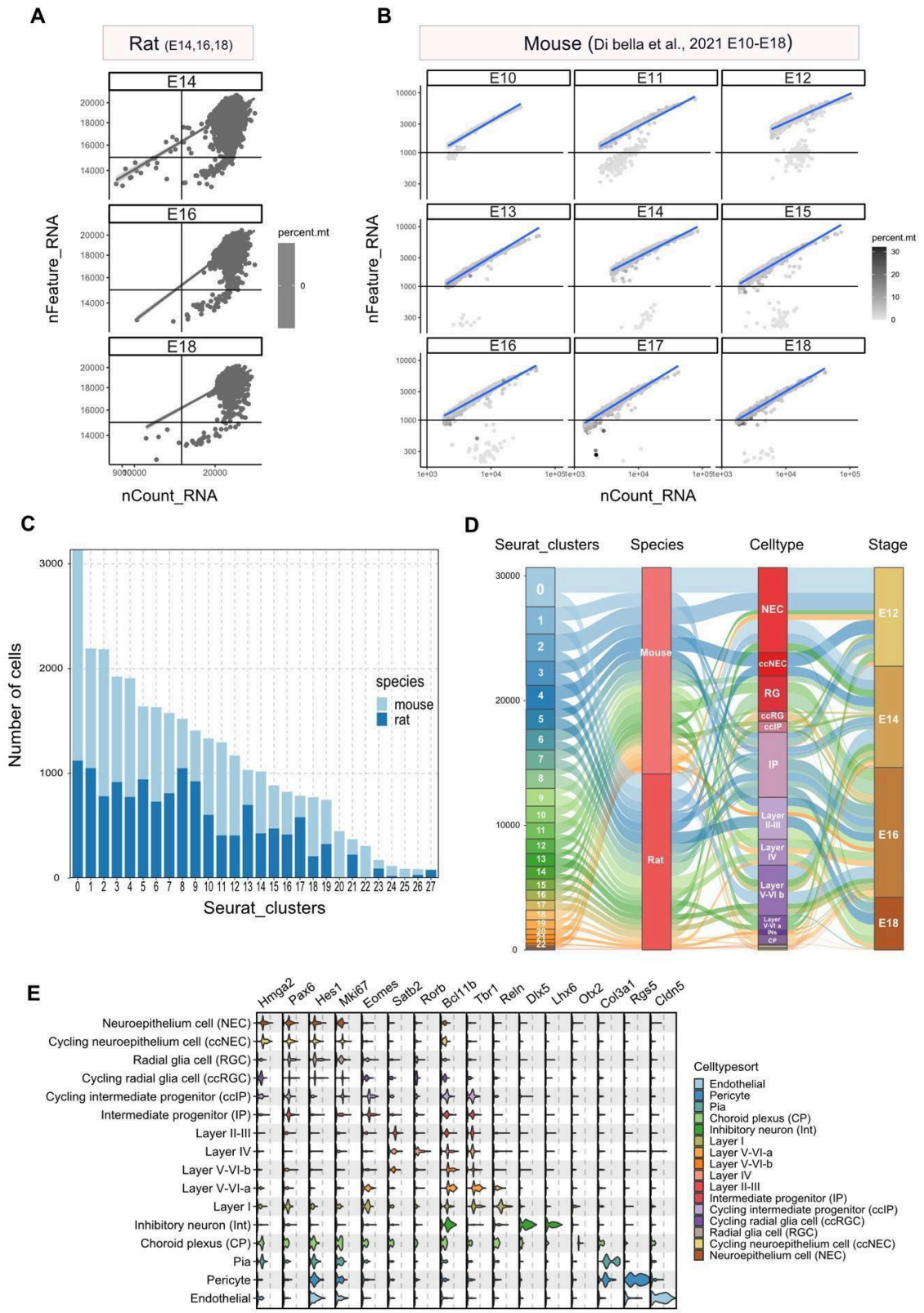

Supplementary Figure S6. Single cell RNA sequencing of mouse and rat cortical cells (**A and B**) Distribution of detected genes, UMI counts, and mitochondrial read percentages in rat (A) and mouse (B) datasets. (**C**) Cell numbers in UMAP clusters for both species. (**D**) Relationship of clusters, species, cell types, and developmental stages. (**E**) Expression of canonical markers in annotated cell types.

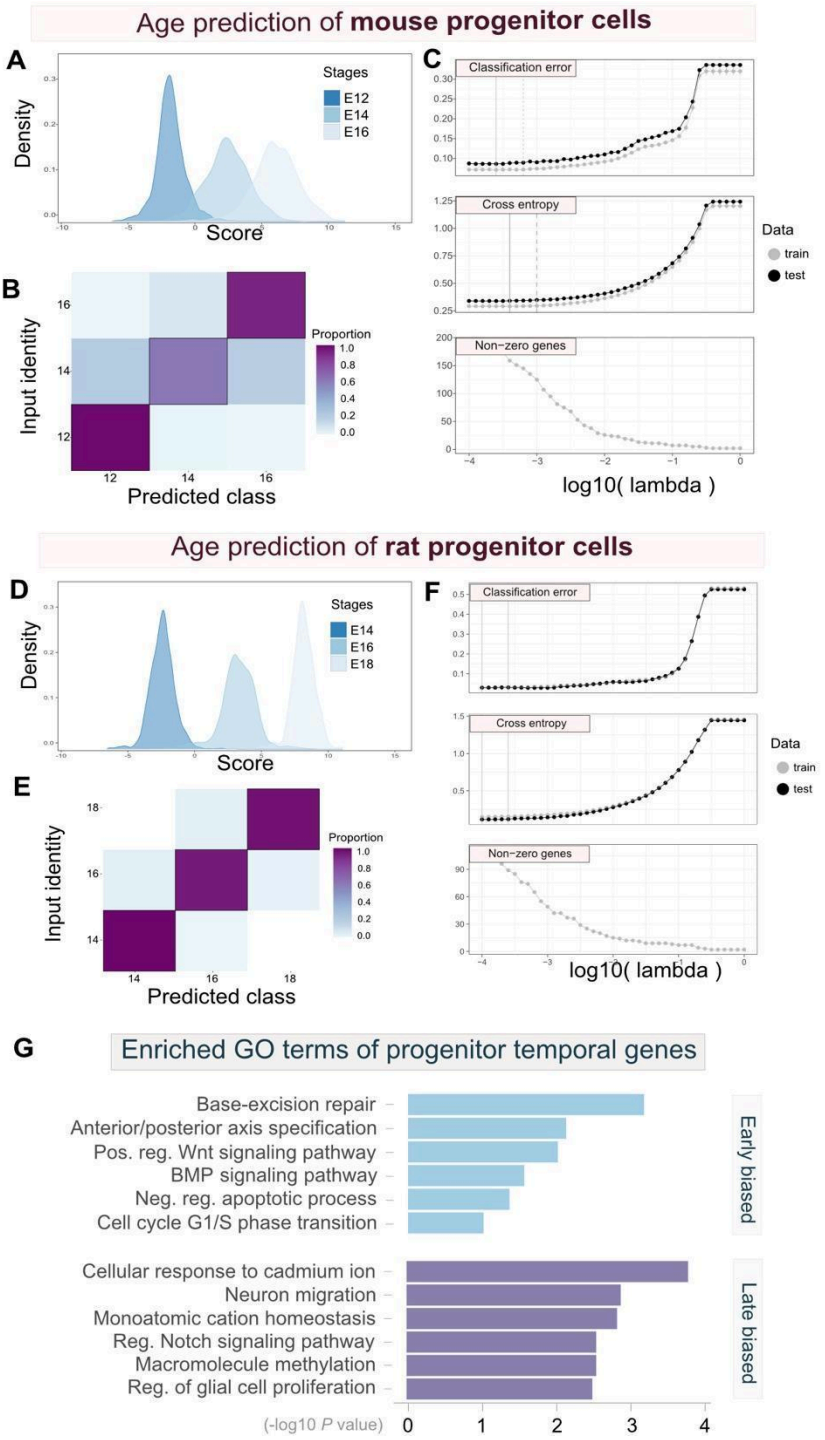

Supplementary Figure S7. Identification of progenitor age genes using the ordinal regression model

(**A** to **F**) Expression of progenitor age genes predicts sampling stages of progenitor cells in mice (A to C) and rats (D to F). (**G**) Gene ontology analysis of progenitor age genes.

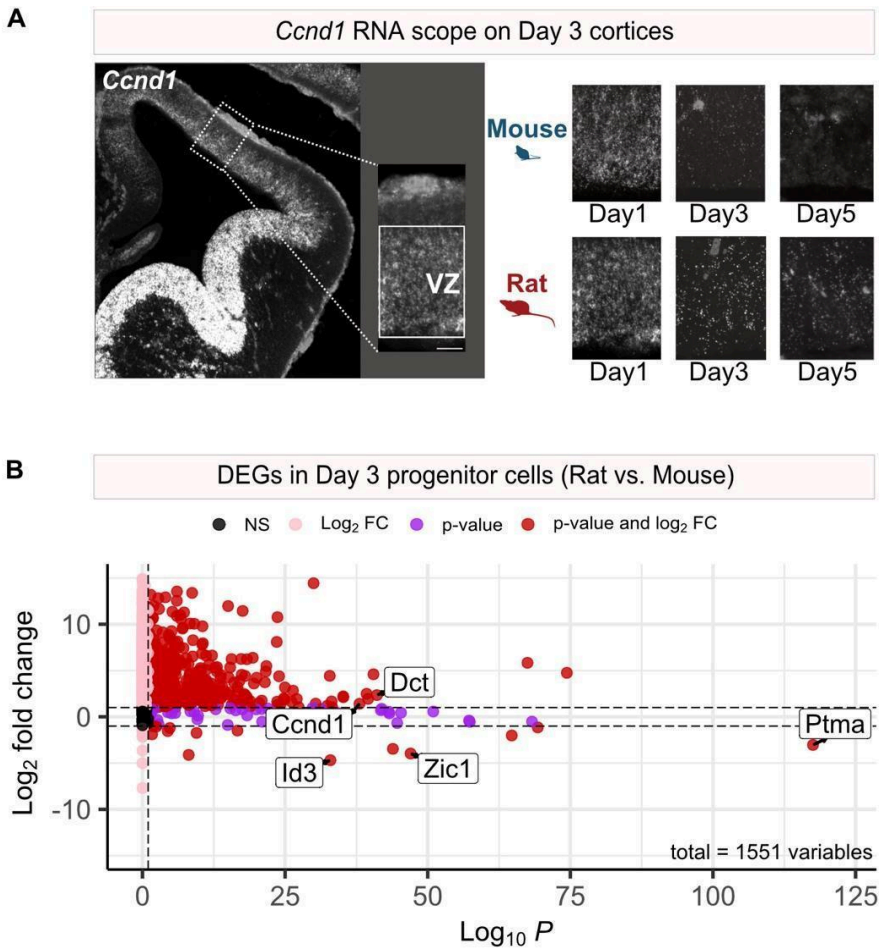

Supplementary Figure S8. Comparison of *Ccnd1* expression in the mouse and rat cortical progenitors during neurogenesis

(**A**) Fluorescent *in situ* hybridization shows differences in *Ccnd1* expression in cortical progenitors during neurogenesis. (**B**) Differential expression analysis identifies significantly enriched genes, including *Ccnd1*, in rat and mouse progenitors at Day 3.

Table S1. List of Primary Antibodies

target	concentration	host species	manufacture	catalog #	RRID
GFP	1:1000	chicken	Abeam	ab13970	AB_300798
RFP	1:1000	rabbit	Rockland	600-401-379	AB_2209751
Vglut2	1:250	rat	Synaptic systems	135403	AB_887883
Ctip2	1:500	rat	Abcam	ab18465	AB_2064130
Satb2	1:500	mouse	Abcam	ab51502	AB_882455
Satb2	1:1000	rabbit	Abcam	ab34735	AB_2301417
Olig2	1:1000	goat	R&D systems	AF2418-SP	AB_2157554
Tbr1	1:1000	rabbit	Abcam	ab183032	AB_2936859
Pax6	1:1000	rabbit	MBL	PD022	AB_1520876
β3tublin	1:1000	mouse	Covance	MMS-435P	AB_2313773
NeuN	1:1000	mouse	Sigma-Aldrich	MAB377	AB_2298772
PH3	1:1000	rat	Abcam	ab10543	AB_2295065
Tbr2	1:500	rabbit	Atlas Antibodies	HPA028896	AB_10601370
Tbr2	1:500	rat	Thermo Fisher	14-4875-82	AB_11042577

Table S2. List of Secondary Antibodies

target	concentration	host species	manufacture	conjugation	catalog #	RRID
chicken IgY (H+L)	1:1000	donkey	Jackson immunoresearch	Alexa fluor 488	703-545-155	AB_2340375
mouse IgG (H+L)	1:1000	donkey	Abcam	Alexa fluor 405	ab175659	N/C
mouse IgG (H+L)	1:1000	donkey	Invitrogen	Alexa fluor 555	A31570	AB_2313501
rat IgG (H+L)	1:1000	donkey	Jackson immunoresearch	Cy3	712-165-153	AB_2340667
rat IgG (H+L)	1:1000	donkey	Invitrogen	Alexa fluor 647	A48272	AB_2893138
goat IgG (H+L)	1:1000	donkey	Invitrogen	Alexa fluor 647	A21447	AB_141844
rabbit IgG (H+L)	1:1000	donkey	Invitrogen	Alexa fluor 488	A21206	AB_2535792
rabbit IgG (H+L)	1:1000	donkey	Invitrogen	Alexa fluor 555	A31572	AB_162543
rabbit IgG (H+L)	1:1000	donkey	Invitrogen	Alexa fluor 647	A31573	AB_2536183